Atmos. Chem. Phys. Discuss., 15, 32185–32238, 2015
www.atmos-chem-phys-discuss.net/15/32185/2015/
doi:10.5194/acpd-15-32185-2015

Atmospheric Chemistry and Physics Discussions

Temporal variations in CO_2 and CO at Ahmedabad in western India

N. Chandra[1,2], S. Lal[1], S. Venkataramani[1], P. K. Patra[3], and V. Sheel[1]

[1]Physical Research Laboratory, Ahmedabad 380009, India
[2]Indian Institute of Technology, Gandhinagar 382355, India
[3]Department of Environmental Geochemical Cycle Research, JAMSTEC, Yokohama 2360001, Japan

Received: 29 September 2015 – Accepted: 4 November 2015 – Published: 17 November 2015

Correspondence to: S. Lal (shyam@prl.res.in)

Published by Copernicus Publications on behalf of the European Geosciences Union.

Abstract

About 70 % of the anthropogenic CO_2 is emitted from the megacities and urban areas of the world. In-situ simultaneous measurements of carbon dioxide (CO_2) and carbon monoxide (CO) have been made using a state-of-the-art laser based cavity ring down spectroscopy technique at Ahmedabad, an urban site in western India, from November 2013 to May 2015 with a break during March to June 2014. Annual average concentrations of CO_2 and CO have been found to be 413.0 ± 13.7 ppm and 0.50 ± 0.37 ppm respectively. Both the species show strong seasonality, with lower concentrations of 400.3 ± 6.8 ppm and 0.19 ± 0.13 ppm, respectively during the south-west monsoon, and higher values of 419.6 ± 22.8 ppm and 0.72 ± 0.68 ppm, respectively in autumn (SON). Strong diurnal variations are also observed for both the species. The common factors for diurnal cycles of CO_2 and CO are the vertical mixing and rush hour traffic, while the influence of biospheric fluxes is also seen in CO_2 diurnal cycle. Using CO and CO_2 covariation, we differentiate the anthropogenic and biospheric components of CO_2 and found that significant contributions of biospheric respiration and anthropogenic emission in the late night (00:00–05:00 IST) and evening rush hours (18:00–22:00 IST) respectively. We compute total yearly emission of CO to be 69.2 ± 0.07 Gg for the study region using the observed CO : CO_2 correlation slope and bottom-up CO_2 emission inventory. This calculated emission of CO is 52 % larger than the estimated emission of CO by the EDGAR inventory. The observations of CO_2 have been compared with an atmospheric chemistry transport model (i.e., ACTM), which incorporates various components of CO_2 fluxes. ACTM is able to capture the basic variabilities, but both diurnal and seasonal amplitudes are largely underestimated compared to the observations. We attribute this underestimation by model to uncertainties in terrestrial biosphere fluxes and coarse model resolution. The fossil fuel signal from the model shows fairly good correlation with observed CO_2 variations, which supports the overall dominance of fossil fuel emissions over the biospheric fluxes in this urban region.

ACPD
15, 32185–32238, 2015

1 Introduction

Carbon dioxide (CO_2) is the most important anthropogenically emitted greenhouse gas (GHG) and has increased substantially from 278 to 390 ppm in the atmosphere since the beginning of the industrial era (circa 1750). It has contributed to more than 65 % of the radiative forcing increase since 1750 and hence leads to the significant impact on the climate system (Ciais et al., 2013). Major causes of CO_2 increase are anthropogenic emissions, especially fossil fuel combustion, cement production and land use change. The cumulative anthropogenic CO_2 emissions from the preindustrial era to 2011, are estimated to be 545 ± 85 Pg C, out of which fossil fuel combustion and cement production contributed 365 ± 30 Pg C and land use change (including deforestation, afforestation and reforestation) contributed 180 ± 80 Pg C (Ciais et al., 2013). Land and oceans are the two important sinks of atmospheric CO_2, which remove about half of the anthropogenic emissions (Le Quéré et al., 2014). Though the global fluxes of CO_2 can be estimated fairly well, the regional scale (e.g. sub-continent and country level) fluxes are associated with quite high uncertainty especially over South Asian region; the estimation uncertainty being larger than the value itself (Patra et al., 2013; Peylin et al., 2013). Detailed scientific understanding of the flux distributions is needed for formulating effective mitigation policies (such as Kyoto Protocol). In inverse modelling, CO_2 flux is estimated from atmospheric CO_2 observations and using an atmospheric transport model. Therefore, it is necessary to measure CO_2 concentrations covering different ecosystems and geographical areas of the world, which unfortunately is not the case (Gurney et al., 2002).

Although, carbon monoxide (CO) is not a direct GHG but it affects climate and air quality through the formation of CO_2 and ozone (O_3). It affects the oxidizing capacity of the atmosphere through reaction with the free OH radicals. Additionally, CO can be used as a surrogate tracer for detecting and quantifying anthropogenic emissions from burning processes, since it is a major product of incomplete combustion (Turnbull et al., 2006; Wang et al., 2010). The vehicular emissions contribute large fluxes of CO_2 and

ACPD
15, 32185–32238, 2015

CO to the atmosphere in urban regions. The verification of future mitigation activities demand for quantifying the spatiotemporal distributions of these emissions. The CO emissions have large uncertainty as compared to CO_2, because its emission strongly depends on the combustion efficiency, the vehicle engine and their adopted technology as well as driving conditions. The correlation slope between the atmospheric variations of CO and CO_2 can be used to quantify the fossil fuel contribution, distinguish between different burning processes or to determine the burning efficiency and overall trend of anthropogenic emissions of CO in a city (Turnbull et al., 2006; Wunch et al., 2009; Newman et al., 2013; Popa et al., 2014). The $CO : CO_2$ ratios are higher for low combustion sources (e.g. forest fires) and lower for good or efficient combustion sources (Andreae and Merlet, 2001; Wang et al., 2010). Further, the $CO : CO_2$ ratio can be used for estimating the total emission of CO over an urban area provided the total CO_2 emission is known for that area. Hence, the information about $CO : CO_2$ ratio will be helpful to understand the effects on the CO emissions after adopting the newer vehicular technologies and new cleaner emission norms and finally will be beneficial for reducing the uncertainties in CO emission inventories. Several ground based and aircraft based correlation studies of $CO : CO_2$ have been done in the past from different parts of the world (Turnbull et al., 2006; Wunch et al., 2009; Wang et al., 2010; Newman et al., 2013) but such study has not been done in India except recently reported results from weekly samples for three Indian sites by Lin et al. (2015).

India is the second largest populous country in the world having about 1.3 billion inhabitants. Rapid socioeconomic developments and urbanization have made it the third largest CO_2 emitter next to China and USA since 2011 but it ranks at 137th level based on the per capita emission rate of CO_2 (EDGAR v4.2; CDIAC – Boden et al., 2015). For example, in 2010 India's emission rate was $2.2\,t\,CO_2\,eq\,capita^{-1}$ while the developed countries like USA, Russia and UK had emission rates of about 21.6, 17.6 and $10.9\,t\,CO_2\,eq\,capita^{-1}$ respectively (EDGAR v4.2). The budgets of these gases on regional as well as global scales can be estimated by bottom-up and top down approaches. Large uncertainties are associated in the GHGs budgets over South Asia,

ACPD
15, 32185–32238, 2015

especially over India than for other continents. Based on the atmospheric CO_2 inversion using model calculations, Patra et al. (2013) found that the biosphere in South Asia acted as the net CO_2 sink during 2007–2008 and estimated CO_2 flux of about $-104 \pm 150\,Tg\,C\,yr^{-1}$. Further, based on the bottom-up approach, Patra et al. (2013) gave an estimate of biospheric flux of CO_2 of about $-191 \pm 193\,Tg\,C\,yr^{-1}$ for the period of 2000–2009. Both these approaches show the range of uncertainty 100–150 %. One of the major sources of these large uncertainties is the lack of spatial and temporal observations of these gases (Law et al., 2002; Patra et al., 2013).

The first observations of CO_2, CO and other greenhouse gases started in February 1993 from Cape Rama (CRI) on the south-west coast of India using flask samples (Bhattacharya et al., 2009). After that, several other groups have initiated the measurements of surface level greenhouse gases (Mahesh et al., 2014; Sharma et al., 2014; Tiwari et al., 2014; Lin et al., 2015). Most of these measurements are made at weakly or fortnightly time intervals or at lower accuracy. These data are very useful for several studies like analyzing seasonal cycle, growth rate, and estimating the regional (subcontinental) carbon sources and sinks after combining their concentrations with inverse modelling and atmospheric tracer transport models. However, some important studies like their diurnal variations, temporal covariance ... etc. are not possible from these measurements due to their limitations. Analysis of temporal covariance of atmospheric mixing processes and variation of flux on shorter timescales, e.g., sub-daily, is essential for understanding local to urban scale CO_2 flux variations (Ahmadov et al., 2007; Pérez-Landa et al., 2007; Briber et al., 2013; Lopez et al., 2013; Ammoura et al., 2014; Ballav et al., 2015). Two aircraft based measurements programs namely, Civil Aircraft for the regular Investigation of the atmosphere Based on an Instrument Container (CARIBIC) (Brenninkmeijer et al., 2007) and Comprehensive Observation Network for TRace gases by AIrLiner (CONTRAIL) (Machida et al., 2008) have provided important first look on the South Asian CO_2 budget, but these data have their own limitations (Patra et al., 2011; Schuck et al., 2010, 2012). The focus of the Indigenous research is lacking in terms of making the continuous and simultaneous measurements of CO_2

ACPD
15, 32185–32238, 2015

and CO over the urban regions, where variety of emission sources influence the level of these gases.

Simultaneous continuous measurements of CO_2 and CO have been made since November 2013 from an urban site Ahmedabad located in the western India using very highly sensitive laser based technique. The preliminary results of these measurements for one month period have been reported in (Lal et al., 2015). These detailed measurements are utilized for studying the temporal variations (diurnal and seasonal) of both gases, their emissions characteristics on diurnal and seasonal scale using their mutual correlations, estimating the contribution of vehicular and biospheric emission components in the diurnal cycle of CO_2 using the ratios of CO to CO_2 and rough estimate of the annual CO emissions from study region. Finally, the measurements of CO_2 have been compared with simulations using an atmospheric chemistry-transport model to discuss roles of various processes contributing to CO_2 concentrations variations.

2 Site description, local emission sources and meteorology

The measurement facility is housed inside the campus of the Physical Research Laboratory (PRL), situated in the western part of Ahmedabad (23.03° N, 72.55° E, 55 m a.m.s.l.) in the Gujarat state of India (Fig. 1). It is a semi-arid, urban region in western India, having a variety of large and small scale industries (Textile mills and pharmaceutical production facilities) in east and north outskirts. The institute is situated about 15–20 km away from these industrial areas. The western part is dominated by the residential areas. The city has a population of about 5.6 million (Census India, 2011) and has large number of automobiles (about 3.2 million), which are increasing at the rate of about 10 % yr^{-1}. Most of the city buses and auto-rickshaws (three-wheelers) use compressed natural gas (CNG) as a fuel. The transport-related activities are the major contributors of various pollutants (Mallik et al., 2015). The Indo-Gangetic Plain (IGP) is situated in the northeast of Ahmedabad, which is very densely populated region and has high levels of pollutants emitted from various industries and power plants

ACPD
15, 32185–32238, 2015

along with anthropogenic emissions from burning of fossil fuels and traditional biofuels (wood, cow-dung cake etc). The Thar Desert and the Arabian Sea are situated in the northwest and southwest of Ahmedabad respectively.

Figure 1 shows average monthly variability of temperature, relative humidity (RH), wind speed based on data taken from Wunderground (http://www.wunderground.com), rainfall from Tropical Rainfall Measuring Mission (TRMM) and planetary boundary layer (PBL) height from the Modern-Era Retrospective Analysis for Research and Applications (MEERA). The wind rose plot shows the surface level wind speed and direction during different seasons over Ahmedabad in 2014. This place is known for its semi-arid climate. Large seasonal variations are observed in the wind speed and direction over Ahmedabad. During monsoon (June–July–August), the inter-tropical convergence zone (ITCZ) moves northward across India. It results in the transport of moist and cleaner marine air from the Arabian Sea and the Indian Ocean to the study location by south westerly winds, or the so-called southwest monsoon (summer monsoon). The first shower due to the onset of the southwest monsoon occurs in July and it retreats in the mid of September over Ahmedabad. Due to heavy rain and winds mostly from oceanic region, RH shows higher values in July, August and September. Highest RH of about 83 % is observed in September. The long-range transport of air masses from the northeast part of the Asian continent starts to prevail over the Indian region when ITCZ moves back southward in September and October. These months are regarded as transition period for the monsoon. During autumn (September–October–November), the winds are calm and undergo a change in their direction from south west to north east. When the transition of winds takes placed from oceanic to continental region in October, the air gets dryer and RH decreases until December. The winds are north easterly during winter (December- January–February) and transport pollutants mostly from continental region (IGP region). During pre-monsoon season (March–April–May), winds are north westerly and little south westerly which transport mixed air masses from continent and oceanic regions. The average wind speed is observed higher in June and July while lower in October and March when transition of wind starts from

ACPD
15, 32185–32238, 2015

oceanic to continental and continental to oceanic respectively. The monthly averaged temperature starts increasing from January and attains maximum (34.6 ± 1.4 °C) in June, followed by a decrease until September and temperature is slightly warmer in October compared to the adjacent months. The monthly variation in planetary boundary layer height (PBLH) closely resembles with the temperature pattern. Maximum PBLH of about 1130 m is found in June and it remains in the lower range at about 500 m during July to January. The ventilation coefficient (VC) is obtained by multiplying wind speed and PBL height which gradually increases from January to attain the maximum value in June and the lowest values of VC are observed in October and November.

3 Experiment and model details

3.1 Experimental method

The measurements of ambient CO_2 and CO are performed using a Picarro-G2401 instrument, which is based on the wavelength scanned cavity ring down spectroscopic (CRDS) technique. CRDS is now a well-established technique for making high-sensitivity and high precision measurements of trace gases in the ambient air, due to its three main characteristics (Bitter et al., 2005; Chen et al., 2010; Karion et al., 2013). First, it provides very long interaction path length (around 20 km) between the sample and the incident wavelength, by utilizing a 3-mirror configuration, which enhances its sensitivity over other conventional techniques like Non-dispersive Infrared Spectroscopy (NDIR) and Fourier Transform Infrared Spectroscopy (FTIR). The second is its ability to isolate a single spectral feature with a resolution of 0.0003 cm^{-1}, which ensures that the peak height or area is linearly proportional to the concentration. The third advantage is that the measurements of trace gases using this technique are achieved by measuring the decay time of light intensity inside the cavity while the conventional optical absorption spectroscopy technique is based on absorption of light intensity. Hence, it increases the accuracy of measurements because it is insensitive

ACPD
15, 32185–32238, 2015

to the fluctuations of incident light. The precision and accuracy of these measurements follow the WMO compatibility goals of ±0.1 ppm CO_2 and ±2 ppb CO.

Figure 2 shows the schematic diagram of the measurement system, which consists of the analyser, a glass bulb, a Nafion dryer, a heatless dryer, other associated pumps and a set of calibration mixtures. Atmospheric air is sampled continuously from the terrace of the building (20 m above the ground level) through an 1/4 inch PFA Teflon tube via a glass manifold. An external pump is attached on one side of the glass manifold to flush the sample line. Water vapor affects the measurements of CO_2 by diluting its mixing ratios in the air and by broadening the spectroscopic absorption lines of other gases. Although, the instrument has ability to correct for the water vapour interferes by using an experimentally derived water vapor correction algorithms (Crosson, 2008), but it has an absolute H_2O uncertainty of ~ 1 % (Chen et al., 2010) and can introduces a source of error using a single water vapor correction algorithm (Welp et al., 2013). This error can be minimized by either generating the correction coefficients periodically in the laboratory or by removing the water vapour from the sample air. Conducting the water vapor correction experiment is bit tricky and need extra care as discussed by Welp et al. (2013). Hence, we prefer to remove water vapour from the sample air by introducing a 50-strand Nafion dryer (Perma Pure, p/n PD-50T-24MSS) in the upstream of the analyser. Nafion dryer contains a bunch of semi-permeable membrane tubing separating an internal sample gas stream from a counter sheath flow of dry gas in stainless steel outer shell. The partial pressure of water vapour in the sheath air should be lower than the sample air for effectively removing the water vapour from the sample air. A heatless dryer generates dry air using a 4 bar compressor (KNF, MODEL: NO35ATE) which is used as a sheath flow in Nafion dryer. After drying, sample air passes through the PTFE filter (polytetrafluoroethylene; 5 µm Sartorius AG, Germany) before entering the instrument cavity. This setup dries the ambient air near to 0.03 % (300 ppm) concentration of H_2O. The CO_2 concentrations are reported on the WMO scale, using the three calibration mixtures of CO_2 ($350.67 \pm 0.02, 399.68 \pm 0.002$ and 426.20 ± 0.006 ppm) from NOAA, Bolder USA, while the concentration of CO is re-

ACPD
15, 32185–32238, 2015

ported against a calibration mixture of CO (970 ppb) from Linde UK. An additional gas standard tank (CO_2: 338 ppm, CO: 700 ppm), known as the "target", is used to determine the precision of the instrument. The target tank values are calibrated against the CO_2 and CO calibration mixtures. The target gas is introduced in the instrument for a period of 24 h. For CO_2 and CO, the 5 min precisions were found to be 0.015 and 0.005 ppm respectively within 1σ. Maximum drift for 24 h has been calculated by subtracting the maximum and minimum value of 5 min average which were found to be 0.2 and 0.015 ppm respectively for CO_2 and CO. The linearity of the instrument for CO_2 measurements has been checked by using three calibration standards (350.67, 399.68 and 426.20 ppm) of CO_2. The linearity tests are conducted very frequently and the slope is found in the range of 0.99–1.007 ppm with correlation coefficient (r) of about 0.999.

3.2 Description of AGCM-based Chemistry Transport Model (ACTM)

This study uses the Center for Climate System Research/National Institute for Environmental Studies/Frontier Research Center for Global Change (CCSR/NIES/FRCGC) atmospheric general circulation model (AGCM)-based chemistry-transport model (ACTM). The model is nudged with reanalysis meteorology using Newtonian relaxation method. The U and V components of horizontal winds are used from the Japan Meteorological Agency Reanalysis (JRA-25) (Onogi et al., 2007). The model has $1.125^\circ \times 1.125^\circ$ horizontal resolution (T106 spectral truncation) and 32 vertical sigma-pressure layers up to about 50 km. Three components namely anthropogenic emissions, monthly varying ocean exchange with net uptake and terrestrial biospheric exchange of surface CO_2 fluxes are used in the model. The fossil fuel emissions for the model simulations are taken from EDGAR inventory for the year of 2010. Air-sea fluxes from Takahashi et al. (2009) have been used for the oceanic CO_2 tracer. The oceanic fluxes are monthly and are linearly interpolated between mid-months. The terrestrial biospheric CO_2 tracers are provided from the Carnegie-Ames-Stanford-Approach (CASA) process model (Randerson et al., 1997), after introducing a diurnal

ACPD
15, 32185–32238, 2015

variability using 2 m air temperature and surface short wave radiation from the JRA-25 as per Olsen and Randerson (2004). The ACTM simulations has been extensively used in TransCom CO_2 model inter-comparison studies (Law et al., 2008; Patra et al., 2008).

4 Results and discussion

4.1 Time series and general statistics

Figure 3a and c shows the time series of 30 min average CO_2 and CO concentrations for the period of November 2013–February 2014 and July 2014 to May 2015. The concentrations of both gases exhibit large synoptic variability because the site is close to anthropogenic sources. The concentrations and variability of both gases are observed lowest in the month of July and August. Maximum scatter in the concentrations and several plumes of very high levels both gases have been observed from October 2014 until mid-March 2015. Almost all plumes of CO_2 and CO are one to one correlated and are found during evening rush hours and late nights. Figure 3e and f shows the variations of CO_2 and CO concentrations with wind speed and direction for the study period except July, August and September due to non-availability of wind data. Most of the high and low concentrations of both these gases are found to be associated with low and high wind speeds. There is no specific direction for high levels of these gases. This probably indicates the transport sector is an important contributor to the local emissions since the measurement site is surrounded by city roads.

Figure 3b and d shows the probability distributions or frequency distributions of CO_2 and CO concentrations during the study period. The frequency distribution of CO_2 shows almost normal distribution while CO shows skewed towards right (lower concentrations). This is because, natural cycle of the biosphere (photosynthesis and respiration) along with some common controlling factors (local meteorology and anthropogenic sources), affects significantly the levels of CO_2. The control of the boundary

ACPD
15, 32185–32238, 2015

layer is common for the diurnal variations of these species because of their chemical lifetimes are longer (> months) than the timescale of PBL height variations (~ h). However, biospheric fluxes of CO_2 can have strong hourly variations. During the study period the CO_2 concentrations varied between 382–609 ppm, with 16 % of data lying below 400 ppm, 50 % lying in the range 400–420 ppm, 25 % between 420–440 ppm and 9 % in the range of 440–570 ppm. Maximum frequency of CO_2 is observed at 402.5 ppm during the study period. The CO concentrations lies in the range of 0.071–8.8 ppm with almost 8 % data lies below the most probable frequency of CO at 0.2 ppm, while 70 % data lies between the concentrations of 0.21 and 0.55 ppm. Only 8 % data lies above the concentration of 1.6 ppm and rest of 14 % data lies between 0.55 and 1.6 ppm. The annual mean concentrations of CO_2 and CO are found to be 413.0 ± 13.7 ppm and 0.50 ± 0.37 ppm respectively, after removing outliers beyond 2σ values.

4.2 Seasonal variations of CO_2 and CO

The seasonal cycles of CO_2 and CO are mostly governed by the strength of emission sources, sinks and transport patterns. Although they follow almost identical seasonal patterns but the factors responsible for their seasonal behaviours are distinct as for the diurnal variations. We calculate the seasonal cycle of CO_2 and CO using two different approaches. In first approach, we use monthly mean of all data and in the second approach we use monthly mean for afternoon period (12:00–16:00 IST) only. All times are in Indian Standard Time (IST), which is 5.5 h ahead of GMT. The seasonal cycle from first approach depicts the combined influence of local emissions (mostly) as well as that of large scale circulation. The second approach removes the auto-covariance by excluding CO_2 and CO data mainly affected by local emission sources and represent seasonal cycles at the well mixed volume of the atmosphere. The CO_2 time series is detrended by subtracting a mean growth rate of CO_2 observed at Mauna Loa (MLO), Hawaii, i.e., 2.13 ppm yr^{-1} or 0.177 ppm $month^{-1}$ (www.esrl.noaa.gov/gmd/ccgg/trends/) for clearly depicting the seasonal cycle ampli-

ACPD
15, 32185–32238, 2015

tude. Figure 4a and b shows the variations of monthly average concentrations of CO_2 and CO using all daily (00:00–24:00 IST) data and afternoon (12:00–16:00 IST) data.

Both average concentrations (total and noon time) of CO_2 exhibit strong seasonal cycle, but show distinct patterns (occurrence of maxima and minima) to each other. This difference occurs because seasonal cycle of CO_2 from all data is mostly governed by the PBL ventilation and large scale circulation while the seasonal cycle from noon time mean concentration is mostly related to the seasonality of vegetation activity. The total and noon time mean concentrations of CO show almost similar pattern and evince that the seasonal cycle of CO_2 from the afternoon mean is mostly controlled by the biospheric productivity, since biospheric cycle does not influence CO concentration directly. In general, total mean values of CO_2 and CO are observed lower in July having concentration 398.78 ± 2.8 ppm and 0.15 ± 0.05 ppm respectively. A sudden increase in the total mean of both gases is observed from September to October and maximum concentrations of CO_2 and CO are observed to be 424.85 ± 17 ppm and 0.83 ± 0.53 ppm, respectively, during November. From January to May the total mean concentration of CO_2 decreases from 415.34 ± 13.6 to 406.14 ± 5.0 ppm and total mean concentration of CO decreases from 0.71 ± 0.22 to 0.22 ± 0.10 ppm. During monsoon months predominance of south-westerly winds which bring cleaner air from the Arabian Sea and the Indian Ocean over to Ahmedabad and high VC (Fig. 1) are responsible for the lower concentration of total mean of both the gases. CO_2 and CO concentrations are also at their seasonal low in the Northern Hemisphere due to net biospheric uptake and seasonally high chemical loss by reaction with OH, respectively. In addition, deep convections in the southwest monsoon season efficiently transport the Indian emission (for CO, hydrocarbons) or uptake (for CO_2) signals at the surface to the upper troposphere, resulting in concentrations at the surface in the summer compared to the winter months (Kar et al., 2004; Randel and Park, 2006; Park et al., 2009; Patra et al., 2011; Baker et al., 2012). During autumn and early winter (December), lower VC values cause trapping of anthropogenically emitted CO_2 and CO. This is the major cause for high CO_2 and CO concentrations during this period. The north-easterly winds bring

ACPD
15, 32185–32238, 2015

very high levels of pollutants from IGP region and could additionally enhance the levels of CO_2 and CO during these seasons (autumn and winter). Higher VC and predominance of comparatively less polluted mixed air masses from oceanic and continental region results in the lower total mean concentrations of both gases.

There are some clear differences which are observed in the afternoon mean concentrations of CO_2 as compared to daily mean. The first distinct feature is that significant difference of about 5 ppm is observed in the afternoon mean of CO_2 concentration from July to August as compared to difference in total mean concentration of about ~ 0.38 ppm for the same period. Significant difference in the afternoon concentrations of CO_2 from July to August is mainly due to the increasing sink by net biospheric productivity after the Indian summer monsoonal rainfall. Another distinct feature is that the daily mean concentration of CO_2 is found highest in November while the afternoon mean concentration of CO_2 attains maximum value (406 ± 0.4 ppm) in April. Prolonged dry season combined with high daytime temperature (about 41 °C) during April–May make the tendency of ecosystem to become moderate source of carbon exchange (Patra et al., 2011) and this could be responsible for the elevated mean noon time concentrations of CO_2.

The average amplitude (max–min) of the annual cycle of CO_2 is observed around 13.6 and 26.07 ppm from the afternoon mean and total mean respectively. Different annual cycles and amplitudes have been observed from other studies conducted over different Indian stations. Similar to our observations of the afternoon mean concentrations of CO_2, maximum values are also observed in April at Pondicherry (PON) and Port Blair with amplitude of mean seasonal cycles about 7.6 ± 1.4 and 11.1 ± 1.3 ppm respectively (Lin et al., 2015). Cape Rama (CRI), a costal site on the south-west coast of India show the seasonal maxima one month before than our observations in March with annual amplitude about 9 ppm (Bhattacharya et al., 2009). The Sinhagad (SNG) site located over the Western Ghats mountains, show very larger seasonal cycle with annual amplitude of about 20 ppm (Tiwari et al., 2014). The amplitude of mean annual cycle at the free tropospheric site Hanle at altitude of 4500 m is observed to be

ACPD
15, 32185–32238, 2015

8.2±0.4 ppm, with maxima in early May and minima in mid-September (Lin et al., 2015). Distinct seasonal amplitudes and patterns are due to differences in regional controlling factors for the seasonal cycle of CO_2 over these locations, e.g., the Hanle is remotely located from all continental sources, Port Blair site is sampling predominantly marine air, Cape Rama observes marine air in the summer and Indian flux signals in the winter, and Sinhagad represents a forested ecosystem. These comparisons show the need for CO_2 measurements over different ecosystems for constraining its budget.

The annual amplitude in afternoon and daily mean CO concentrations are observed to be about 0.27 and 0.68 ppm, respectively. The mean annual cycles of CO over PON and Port Blair show the maxima in the winter months and minima in monsoon months same as our observations with annual amplitudes of 0.078 ± 0.01 and 0.144 ± 0.016 ppm, respectively. Hence, the seasonal levels of CO are affected by large scale dynamics which changes air masses from marine to continental and vice versa and by photochemistry. The amplitudes of annual cycle at these locations differ due to their climatic conditions and sources/sinks strengths.

4.3 Diurnal variation

The diurnal patterns for all months and seasons are produced by first generating the time series from the 15 min averages and then averaging the individual hours for all days of the respective month and season after removing the values beyond 2σ standard deviations for each month as outliers.

4.3.1 Diurnal variation of CO_2

Figure 5a shows bi-modal feature in the diurnal cycle of CO_2 during the four seasons with morning and evening peaks. Both peaks are associated mostly with the vehicular emissions and PBL height during rush hours. There are many interesting features in the 00:00–08:00 IST period. Concentrations of CO_2 start decreasing from 00:00 to 03:00 IST and afterwards increases until 06:00 and 07:00 IST during monsoon and au-

ACPD
15, 32185–32238, 2015

tumn. It could be mostly due to the accumulation of CO_2 emitted from respiration by the biosphere in the nocturnal boundary layer. During winter and spring the concentrations during night hours are almost constant and increase is observed only from 06:00 to 08:00 IST during winter. Dormant of respiration during these two seasons due to lower temperature could be one of the possible factors for no increase in CO_2 concentrations during night. No peak during morning hours is observed in spring. Distinct timings for the occurrence of the morning peak during different seasons is generally related to the sunrise time and consequently the evolutions of PBL height. The sunrise occurs at 05:55–06:20, 06:20–07:00, 07:00–07:23 and 07:20–05:54 IST during monsoon, autumn, winter and spring, respectively. During spring and monsoon, rush hour starts after sunrise, so the vehicular emissions occur when the PBL is already high and photosynthetic activity has begun. But in winter and autumn rush hour starts parallely with the sunrise, so the emissions occur when the PBL is low and concentration build up is much strong in these seasons than in spring and monsoon seasons. CO_2 starts decreasing fast after these hours and attains minimum value around 16:00 IST. This quick drop of CO_2 after sunrise is linked to the dominance of photosynthesis over the respiration processes in addition to the higher atmospheric mixing height. CO_2 levels start increasing after 16:00 IST peak around 21:00 IST. Higher concentrations of CO_2 during these hours are mainly due to the rush hour vehicular emissions and less dilution due to the lower PBL height. Comparative levels of CO_2 during evening rush hours except monsoon confirm separately the major influence from the same type of sources (vehicular emission) in its levels which do not show large variability as in post-midnight hours.

The diurnal amplitude is defined as the difference between the maximum and minimum concentrations of CO_2 in the diurnal cycle. The amplitudes of monthly averaged diurnal cycle of CO_2 from July 2014 to May 2015 are shown in Fig. 5b. The diurnal amplitude shows large month to month variation with increasing trend from July to October and decreasing trend from October onwards. Lowest diurnal amplitude of about 6 ppm is observed in July while highest amplitude of about 51 ppm is observed in October.

ACPD
15, 32185–32238, 2015

The amplitude does not change much from December to March and is observed in the range of 25–30 ppm. Similarly from April to May, the amplitude also varies in a narrow range from 12 to 15 ppm. The jump in the amplitude of CO_2 diurnal cycle is observed highest (around 208 %) from July to August. This is mainly due to significant increase of biospheric productivity from July to August after the rains in Ahmedabad. It is observed that during July the noon time CO_2 levels are found in the range of 394–397 ppm while in August the noon time levels are observed in the range of 382–393 ppm. The lower levels could be due to the higher PBL height during afternoon and cleaner air, but in case of CO, average day time levels in August are observed higher than July. It rules out that the lower levels during August are due to the higher PBL height and presence of cleaner marine air, and confirms the higher biospheric productivity during August.

The monthly average diurnal cycles of the biospheric net primary productivity from CASA model for Ahmedabad and for the year of 2014 are shown Fig. 6. The details of CASA flux are given in the Sect. 3.2. It is observed that the model shows higher biospheric productivity in September and October while the observations are suggesting higher productivity in August. This indicates that the CASA model is not able to capture the signal of higher biospheric productivity for Ahmedabad and need to be improved. Similar discrepancy in the timing of maximum biospheric uptake is also discussed earlier by Patra et al. (2011) using inverse model CO_2 fluxes and CASA biospheric fluxes.

Near surface diurnal amplitude of CO_2 has been documented in humid subtropical Indian station Dehradun and a dry tropical Indian station Gadanki (Sharma et al., 2014). In comparison to Ahmedabad, both these stations show distinct seasonal change in the diurnal amplitude of CO_2. The maximum CO_2 diurnal amplitude of about 69 ppm is observed during the monsoon season at Dehradun (30.3° N, 78.0° E, 435 m), whereas maximum of about 50 ppm during autumn at Gadanki (13.5° N, 79.2° E, 360 m).

4.3.2 Diurnal variation of CO

Figure 7a shows seasonally averaged diurnal variation of CO. In general, the mean diurnal cycles of CO during all the seasons show lower concentration during noon

ACPD
15, 32185–32238, 2015

(12:00–17:00 IST) and two peaks, one in the morning (08:00–10:00 IST) and other in the evening (18:00–22:00 IST). This cycle exhibits the same pattern as the mean diurnal cycle of traffic flow, with maxima in the morning and at the end of the afternoon, which suggests the influence of traffic emissions on CO measurements. Along with the traffic flow, PBL dynamics also plays a critical role in governing the diurnal cycle of CO. The amplitudes of the evening peaks in diurnal cycles of CO are always greater than the morning peaks. It is because the PBL height evolves side by side with the morning rush hours traffic and hence increased dilution while during evening hours PBL height decrease along with evening time rush hours traffic and favours accumulation of pollutants until the late evening under the stable PBL conditions. The noon time minima is associated with the combined influence of boundary layer dilution and loss of CO due to OH radicals. The peaks during morning and evening rush hours, minima during afternoon hours in CO diurnal cycle during all seasons are similar as in CO_2. However, there are a few noticeable differences in the diurnal cycles of both the gases. The first noticeable difference is that the CO morning peak appears later than CO_2 peak. This is because as discussed earlier with sunrise time, PBL height starts to evolve and same time photosynthesis process also gets started and hence CO_2 morning peak depends on the sunshine time. But in case of CO, timing of the morning peak mostly depends on the rush hour traffic and is consistent at 08:00–10:00 IST in all seasons. The second noticeable difference is the afternoon concentrations of CO show little seasonal spread as compared to the afternoon concentrations of CO_2. Again, this is due to the biospheric control on the concentration of CO_2 during the afternoon hours of different seasons while CO levels are mainly controlled by the dilution during these afternoon hours. The third noticeable difference is that the levels of CO decrease very fast after evening rush hour in all seasons while this feature is not observed in case of CO_2 since respiration during night hours contributes to the levels of CO_2. The average morning (08:00–09:00 IST) peak values of CO are observed minimum (0.18 ± 0.1 ppm) in monsoon and maximum (0.72 ± 0.16 ppm) in winter while its evening peak shows minimum value (0.34 ± 0.14 ppm) in monsoon and maximum (1.6 ± 0.74 ppm) in autumn. The

ACPD
15, 32185–32238, 2015

changes in CO concentrations show large fluctuations from morning peak to afternoon minima and from afternoon minima to evening peak. From early morning maxima to noon minima, the changes in CO concentrations are found in the range of 20–200 % while from noon minima to late evening maxima the changes in CO concentrations are found in the range of 85 to 680 %. Similar diurnal variations with two peaks have also been observed in earlier measurements of CO as well as NO_x at this site (Lal et al., 2000).

The evening peak contributes significantly to the diurnal amplitude of CO. The largest amplitude in CO cycle is observed in autumn (1.36 ppm) while smallest amplitude is observed in monsoon (0.24 ppm). The diurnal amplitudes of CO are observed to be about 1.01 and 0.62 ppm respectively during winter and spring. The monthly diurnal cycle of CO (Fig. 7b) shows minimum (0.156 ppm) amplitude in July and maximum (1.85 ppm) in October. After October the diurnal amplitude keep on decreasing till monsoon.

4.4 Correlation between CO and CO_2

The relationships between CO to CO_2 can be useful for investigating the CO source types and their combustion characteristics in the city region of Ahmedabad. For correlations study, in principle the baseline levels need to be removed from the measured concentrations. Although, the most ideal case of determining the background levels are the continuous measurement of respective gases at a cleaner site. But due to unavailability of measurements at a near by cleaner site, we use the 5th percentile value of CO_2 and CO for each day as a background for corresponding day. The excess CO_2 (CO_{2exc}) and CO (CO_{exc}) above the background for Ahmedabad city, are determined for each day after subtracting the background concentrations from the hours of each day ($CO_{2exc} = CO_{2obs} - CO_{2bg}$, $CO_{exc} = CO_{obs} - CO_{bg}$).

We use robust regression method for the correlation study. It is an alternative to least squares regression method and more applicable for analysing time series data with outliers arising from extreme events (http://www.ats.ucla.edu/stat/stata/dae/rreg.htm). Figure 8a illustrates the correlations between CO_{exc} and CO_{2exc} for the four seasons.

ACPD
15, 32185–32238, 2015

The impact of the possible sources of CO and CO_2 varies from month to month and hence season to season. The lowest correlation ($r = 0.62, p = 0.0001$) is observed during monsoon, with a $\Delta CO_{exc}/\Delta CO_{2exc}$ ratio of 0.6 ± 0.1 ppb ppm^{-1}. Lowest correlation suggest that different mechanisms control the levels of CO and CO_2 during the monsoon season. As discussed previously, higher biospheric productivity during this season mostly controls the CO_2 concentrations while CO concentrations are mostly controlled by the long range transport and higher loss due to OH. Highest correlation ($r = 0.87, p < 0.0001$) with $\Delta CO_{exc}/\Delta CO_{2exc}$ ratio of 8.4 ± 0.17 ppb ppm^{-1} is observed during spring season. As illustrated by the diurnal cycle, the CO_2 is not significantly removed by the biosphere during spring with lower draw down in daily CO_2. Along with this, higher VC during this season will result in very fast mixing. Therefore, very fast mixing will mostly regulate their relative variation and will result in higher correlation in this season. Other factors like soil and plant respiration during this period may also control CO_2 concentrations due to which the correlation coefficient is not equal to 1. The ratio of $\Delta CO_{exc}/\Delta CO_{exc}$ is estimated to be 8.5 ± 0.15 ppb ppm^{-1} ($r = 0.72$) and 12.7 ± 0.17 ppb ppm^{-1} ($r = 0.74$) in autumn and winter respectively. Relatively higher ratios during winter than other three seasons indicate contribution of CO emission from additional biofuel burning sources. The winter time ratio is similar to the airmass influenced by both fossil fuel and biofuel emissions as discussed by Lin et al. (2015) over Pondicherry. Using CARIBIC observations, Lai et al. (2010) also reported the $\Delta CO/\Delta CO_2$ ratio in the range of 15.6–29.3 ppb ppm^{-1} from the airmass influenced by both biofuel and fossil fuel burning in the Indo-Chinese Peninsula. Further, $\Delta CO/\Delta CO_2$ ratio is also observed of about 13 ppb ppm^{-1} in South-east Asian outflow in February–April 2001 during the TRACE-P campaign and suggest the combined influence of fossil fuel and biofuel burning (Russo et al., 2003). The narrow range of the ratios from autumn to spring (8.4–12.7 ppb ppm^{-1}) suggest the dominance of local emission sources during these seasons, and this range corresponds to the range of anthropogenic combustion sources (10–15 ppb ppm^{-1}) in developed countries (Suntharalingam et al., 2004; Takegawa et al., 2004; Wada et al., 2011). This suggest that

ACPD
15, 32185–32238, 2015

the overall emissions of CO over Ahmedabad are mostly dominated by the anthropogenic combustion during these seasons.

The $\Delta CO_{exc}/\Delta CO_{2exc}$ slope and their correlation may depend on the time of the day due to the variation in different controlling factors on their levels. Hence, we computed the diurnal cycle of $\Delta CO_{exc}/\Delta CO_{2exc}$ slope for all the seasons by binning the data for both hour and month (3 month × 24 h) as shown in Fig. 8b. The colours indicate the correlation coefficients (r) for respective hour. These ratios do not reflect the diurnally varying PBL height, but rather the diurnally varying mix of fossil fuels and biogenic sources. The $\Delta CO_{exc}/\Delta CO_{2exc}$ slopes show very distinctive diurnal variation, being higher (30–50 ppb ppm^{-1}) in the evening rush hours with very good correlation ($r >$ 0.85) and lower (5–20 ppb ppm^{-1}) in the afternoon hours with lower correlation (r = 0.5–0.6) during all the four seasons. Negative and lower slopes in afternoon hours during monsoon season indicate higher biospheric productivity during this period. The slopes and their correlations are fairly comparable for all the four seasons in the evening rush hours which indicate stronger influence of common emission sources. Slopes during this time can be considered as fresh emissions since dilution and chemical loss of CO can be considered negligible for this time. These observed ratios are much lower than ratios related to domestic sources but are similar transport sector mostly dominated from gasoline combustion (Table 1). Except monsoon, the overall ratios in all four seasons were found in the range of 10–25 ppb ppm^{-1} during the daytime and 10–50 ppb ppm^{-1} during night-time.

4.5 Top-down CO emissions from observations

If the emissions of CO_2 are known for study locations, the emissions of CO can be estimated by multiplying the correlation slopes and molecular mass mixing ratios (Wunch et al., 2009; Wong et al., 2015). Final emissions of CO will depend on choosing the values of correlation slopes. The slopes should not be biased from particular local sources, chemical processing and PBL dynamics. We exclude monsoon data as the CO_2 variations mainly depend on the biospheric productivity during this season. As

ACPD
15, 32185–32238, 2015

discussed previously, the morning and evening rush hours data are appropriate for tracking vehicular emissions, while the afternoon data are affected by other environmental factors, e.g., the PBL dynamics, biospheric activity and chemical process. The stable, shallow night-time PBL accumulates emissions since the evening and hence the correlation slope for this period can be used as a signature of the city's emissions. Hence, we calculate the slopes from the data corresponding to the period of 23:00–05:00 IST. Additionally, slopes for morning hours (06:00–10:00 IST), afternoon hours (11:00–17:00 IST), and night hours (18:00–06:00 IST) are also used for estimating the CO emissions to study the difference in the estimation of CO emissions due to choosing different times for slopes. The CO emission (E_{CO}) for Ahmedabad is calculated using the following formula.

$$E_{CO} = \left(\alpha_{CO} \frac{M_{CO}}{M_{CO_2}}\right) E_{CO_2} \quad (1)$$

Where, α_{CO} is the correlation slope of CO_{exc} to CO_{2exc} ppb ppm^{-1}, M_{CO} is the molecular mass of CO in g mol^{-1}, M_{CO_2} is the molecular mass of CO_2 in g mol^{-1} and E_{CO_2} is the CO_2 emission in Gigagram (Gg) over Ahmedabad. The EDGARv4.2 emission inventory reported an annual emissions of CO_2 at $0.1^\circ \times 0.1^\circ$ for the period of 2000–2008 (http://edgar.jrc.ec.europa.eu/overview.php?v=42). It reported an annual CO_2 emission of 6231.6 Gg CO_2 year^{-1} by EDGARv4.2 inventory over the box ($72.3 <$ longitude $< 72.7^\circ$ E, $22.8 <$ latitude $< 23.2^\circ$ N) which contain Ahmedabad coordinates in center of the box. We assume that the emissions of CO_2 are linearly changing with time and using increasing rate of emission from 2005 to 2008, we extrapolate the emission of CO_2 for 2014 over same area. The bottom-up CO_2 emission for the Ahmedabad is thus estimated of about 8368.6 Gg for the year of 2014. Further, for comparing the estimated emission with inventory emissions we extrapolated the CO emissions also for the year of 2014 using same method applied as for CO_2. Further, we assumed same slopes for the year of 2008 and calculate CO emission for that year

ACPD
15, 32185–32238, 2015

also. The slope values for different time period, estimated and inventory emissions of CO using different values of slope are given in Table 2.

The correlation between CO_{exc} and CO_{2exc} for the period of 23:00–05:00 IST is very tight and slope for this period can be considered for estimating the fossil fuel CO emissions for Ahmedabad. Using this slope and based on CO_2 emissions from EDGAR inventory, the estimated fossil fuel emission for CO is observed to be 69.2 ± 0.7 Gg for the year of 2014. The EDGAR inventory underestimates the emission of CO as they give the estimate of about 45.3 Gg extrapolated for 2014. The slope corresponding to the night hours (18:00–06:00 IST) gives the highest estimate of CO. Using all combinations of slopes, the derived CO emissions are larger than the bottom-up EDGAR emission inventory.

4.6 Diurnal tracking of CO_2 emissions

CO has virtually no natural sources in an urban environment except oxidation of hydrocarbons. As we discussed earlier that incomplete combustion of fossil fuels is the main source of CO in urban environments and therefore can be used as a surrogate tracers to attribute CO_2 enhancements to fossil fuel combustion on shorter timescale. Several studies have demonstrated that the ratio of the excess concentrations of CO and CO_2 in background concentrations can be used to determine the fraction of CO_2 from fossil fuels and validated this method using carbon isotope ($\Delta^{14}CO_2$) measurements (Levin et al., 2003; Turnbull et al., 2006, 2011; Lopez et al., 2013; Newman et al., 2013). This quantification technique is more practical, less expensive and less time consuming in comparison to the $^{14}CO_2$ method (Vogel et al., 2010). For performing this analysis, the background concentrations of CO and CO_2 and the emission ratio of CO/CO_2 from anthropogenic emissions are required. The methods for calculating the background concentrations of CO_2 and CO are already discussed in Sect. 4.4. Figure 9a shows the excess diurnal variations of CO_2 above the background levels during different seasons. As discussed in the previous section, the vehicular emissions are major emission sources over the study locations. For calculating the emission ratio of CO/CO_2 from

ACPD
15, 32185–32238, 2015

the vehicular emissions, we used the evening time (19:00–21:00 IST) concentrations of CO_{2exc} and CO_{exc} for whole study period since correlation for this period is very high. The other reason for choosing this time is that there is insignificant contribution of biospheric CO_2 and no chemical loss of CO. We assume that negligible influence of other sources (open biomass burning, oxidation of hydrocarbons) during this period. The emission ratio for this time is calculated to be about 47 ± 0.27 ppb CO ppm^{-1} CO_2 with very high correlation ($r = 0.95$) (Fig. 9b) after excluding those data points, corresponding for which the mean wind speed is greater than 3 m s^{-1} for avoiding the effect of fast ventilation and transport from other sources. The tight correlation imply that there is no substantial difference in the emission ratio of these gases during the measurement period from November 2013 to May 2015. CO_{2exc} and CO_{exc} will be poorly correlated with each other if their emission ratio varies largely with time, assuming the correlation is mainly driven by emissions. Since this ratio is mostly dominated by the transport sector, this analysis will give mainly the fraction of CO_2 from the emissions of transport sector. We define it as $R_{CO/CO_{2veh}}$. The standard deviation shows the uncertainty associated with slope which is very small. The contribution of transport sector (CO_{2Veh}) in the diurnal cycle of CO_2 is calculated using the following formula.

$$CO_{2Veh} = \frac{CO_{obs} - CO_{bg}}{R_{CO/CO_{2veh}}} \quad (2)$$

where CO_{obs} is the observed CO concentration and CO_{bg} is a background CO value. Uncertainty in the CO_{2Veh} is dominated by the uncertainty in the $R_{CO/CO_{2veh}}$ and by the choice of CO_{bg}. The uncertainty in CO_{2Veh} due to the uncertainty in the $R_{CO/CO_{2veh}}$ is about 0.5 % or 0.27 ppm and can be considered negligible. As discussed in Sect. 3, the uncertainty in the measurements of CO_{bg} is very small and also can be considered negligible. Further, the contributions of CO_2 from other major sources are calculated by subtracting the CO_{2Veh} from the excess concentrations of CO_2. These sources are those sources which do not emit significant amount of CO and can be considered mostly as natural sources (respiration), denoted by CO_{2bio}.

ACPD
15, 32185–32238, 2015

The average diurnal cycles of CO_2 above its background for each seasons are shown in (Fig. 9a). The diurnal pattern of CO_{2Veh} (Fig. 9c) reflects the pattern like CO, because we are using constant $R_{CO/CO_{2veh}}$ for all seasons. Overall, this analysis suggests that the anthropogenic emissions of CO_2 from transport sectors during early morning from 06:00 to 10:00 IST varied from 15 to 60 % (4–15 ppm). During afternoon h (11:00–17:00 IST), the vehicular emitted CO_2 varied from 20 to 70 % (1–11 ppm) and during evening rush hours (18:00–22:00 IST), it varies from 50 to 95 % (2–44 ppm). During night/early morning hours (00:00–07:00 IST) respiration contributes from 8 to 41 ppm of CO_2 (Fig. 9d). The highest contributions from 18 to 41 ppm are observed in the autumn from the respiration sources during night hours, since there is more biomass during this season after the South Asian summer monsoon. During afternoon hours, lower biospheric component of CO_2 could be due to a combination of the effects of afternoon anthropogenic emissions, biospheric uptake of CO_2 and higher PBL height.

4.7 Model – observations comparison

4.7.1 Comparison of diurnal cycle of CO_2

We first evaluate the ACTM in simulating the mean diurnal cycle of CO_2 over Ahmedabad by comparing model simulated surface layer mean diurnal cycle of CO_2. The atmospheric concentrations of CO_2 are calculated by adding the anthropogenic component, oceanic component, biospheric component from CASA process model. Figure 10a and b shows the residuals (Hourly mean – daily mean) of diurnal cycles of CO_2 based on the observations and model simulations respectively. Model shows very little diurnal amplitude as compared to observational diurnal amplitude. Larger differences and discrepancies in night time and morning CO_2 concentrations between the model and observations might be contributed by diurnal cycle of the anthropogenic fluxes from local emissions and biospheric fluxes, and uncertainties in the estimation of PBLH by the model. Hence, there is a need for efforts in improving the regional anthropogenic emissions as well as module for estimating the PBL height. It may be pointed

ACPD
15, 32185–32238, 2015

out that the model's horizontal resolution (1.125° × 1.125°) is coarse for analysing local scale observations. However, model is able to capture the trend of the diurnal amplitude, highest in autumn and lowest in monsoon. Figure 10c shows better agreement (r = 0.75) between the monthly change in model and observational diurnal amplitude of CO_2 from monthly mean diurnal cycle however slope (m = 0.17) is very poor. We include the diurnal amplitudes of CO_2 for November and December 2013 also for improving the total number of data points. The model captured the spread in the day time concentration of CO_2 from monsoon to spring with a difference that model shows lower concentration of CO_2 during noon hours in autumn while observations show lowest in monsoon. Most of the atmospheric CO_2 uptake occur following the Southwest monsoon season during July–September (Patra et al., 2011) and as a consequence, we observe the lowest CO_2 concentration from the measurements during this season. But model is not able to capture this feature since CASA biospheric flux (Fig. 6) shows highest productivity in autumn and hence lowest concentrations of CO_2 in autumn during daytime. This also suggest that there is a need for improving the biospheric flux for this region. It should be mentioned here that CASA model used a land use map corresponding the late 1980s and early 1990s, which should be replaced by rapid growth in urbanised area in Ahmedabad (area and population increased by 91 and 42 %, respectively, between 1990 and 2011). The model resolution may be another factor for discrepancy. As Ballav et al. (2012) show that a regional model WRF-CO_2 is able to capture both diurnal and synoptic variations at two closely spaced stations within 25 km. Hence the regional models could be helpful for capturing these variabilities.

4.7.2 Comparison of seasonal cycle of CO_2

Figure 11a shows the performance of ACTM simulating mean seasonal cycle of CO_2 over Ahmedabad by comparing model simulated mean surface seasonal cycle of CO_2. Due to unavailability of data from March 2014 to June 2014 we plotted the monthly average of the year 2015 for same periods for visualizing the complete seasonal cycle of

ACPD
15, 32185–32238, 2015

CO_2. The seasonal cycles are calculated after subtracting the annual mean from each month, and corrected for growth rate using the observations at MLO. For comparison, we use the seasonal cycle calculated from afternoon time average monthly concentrations, since model is not able to capture the local fluctuations and produce better agreements when boundary layer is well mixed. In Table 3 we present the summary of the comparisons of model and observations. The model reproduces the observed seasonal cycle in CO_2 fairly well but with low seasonal amplitude about 4.15 ppm compared to 13.6 ppm observed. Positive bias during monsoon depicts the underestimation of biospheric productivity by CASA model. The root mean square error is observed highest to be 3.21 % in monsoon. For understanding the role of biosphere, we also compared the seasonal cycle of CO_2 from noon time mean data with the seasonal cycle of CO_2 fluxes over South Asia region which is taken from the Patra et al. (2011) where they calculated it using an inverse model by including CARIBIC data and shifted a sink of 1.5 Pg C yr^{-1} from July to August and termed it as "TDI64/CARIBIC-modified". Positive and negative values of flux show the net release and net sink by the land biosphere over the South Asia. This comparison shows almost one to one correlation in the monthly variation of CO_2 and suggest that the lower levels of CO_2 during July, August and higher level in April are mostly due to the moderate source and sink of South Asian ecosystem during these months respectively. Significant correlation ($r = 0.88$) between South Asian CO_2 fluxes and monthly mean CO_2 data for day time only suggest that the day time levels of CO_2 are mostly controlled by the seasonal cycle of biosphere (Fig. 11b).

Separate correlation between individual tracers of model and observed data has been studied to investigate the relative contribution of individual tracer component in the CO_2 variation (Fig. 11b). We did not include the oceanic tracer and observed CO_2 correlation result, since no correlation has been observed between them. The comparison is based on daily mean of entire time series. Correlation between biospheric tracers and observed CO_2 have been found negative. This is because during growing season biospheric sources act as a net sink for CO_2. Correlation of observed CO_2 with

ACPD
15, 32185–32238, 2015

fossil fuel tracer has been observed fairly well (r = 0.75). Hence, individual tracers correlation study also gives the evidence of the overall dominance of fossil flux in overall concentrations of CO_2 over Ahmedabad for entire study period, and by assuming fossil fuel CO_2 emission we can derive meaningful information on biospheric uptake cycle.

This study suggests that the model is able to capture seasonal cycle with lower amplitude for Ahmedabad. However, the model fails to capture the diurnal variability since local transport and hourly daily flux play important roles for governing the diurnal cycle and hence there is a need for improving these features of the model.

5 Conclusions

We report simultaneous in-situ measurements of CO_2 and CO concentrations in the ambient air at Ahmedabad, a semiarid urban region in western India using laser based CRDS technique during 2013–2015. The unique flow of air masses originating from both polluted continental regions as well as cleaner marine regions over the study location during different seasons make this study most important for studying the characteristics of both polluted and relatively cleaner air masses. Several key results are presented in this study. The observations show the range of CO_2 concentrations from 382 to 609 ppm and CO concentrations from 0.07 to 8.8 ppm, with the average of CO_2 and CO to be 416 ± 19 ppm and 0.61 ± 0.6 ppm respectively. The highest concentrations of both the gases are recorded for lower ventilation and for winds from north-east direction, representing CO_2 and CO transported from anthropogenic sources. The lowest concentrations of both the gases are observed for higher ventilation and for the south-west direction, where air travels from the Indian Ocean. Along with these factors, the biospheric seasonal cycle (photosynthesis outweighs respiration during growing season and reverse during fall season) also controls the seasonal cycle of CO_2. Lowest day time CO_2 concentrations ranging from 382 to 393 ppm in August, suggest for the stronger biospheric productivity during this month over the study region, in agreement with an earlier inverse modelling study. This is in contrast to the terrestrial flux simu-

ACPD
15, 32185–32238, 2015

lated by the CASA ecosystem model, showing highest productivity in September and October months. Hence, the seasonal cycles of both the gases reflect the seasonal variations of natural sources/sinks, anthropogenic emissions and seasonally varying atmospheric transport. The annual amplitudes of CO_2 variation after subtracting the growth rate based on the Mauna Loa, Hawaii data are observed to be about 26.07 ppm using monthly mean of all the data and 13.6 ppm using monthly mean of the afternoon period (12:00–16:00 IST) data only. Significant difference between these amplitudes suggests that the annual amplitude from afternoon monthly mean data only does not give true picture of the variability. It is to be noted that most of the CO_2 measurements in India are based on day time flask samplings only.

Significant differences in the diurnal patterns of CO_2 and CO are also observed, even though both the gases have major common emission sources and effects of PBL dynamics and advection. Differences in their diurnal variability is probably the effect of terrestrial biosphere on CO_2 and chemical loss of CO due to reaction with OH radicals. The morning and evening peaks of CO are affected by rush hours traffic and PBL height variability and occur almost same time throughout the year. However, the morning peaks in CO_2 changes its time slightly due to shift in photosynthesis activity according to change in sun rise time during different seasons. The amplitudes of annual average diurnal cycles of CO_2 and CO are observed about 25 and 0.48 ppm respectively (Table 4). Both gases show highest amplitude in autumn and lowest in monsoon. This shows that major influencing processes are common for both the gases, specific to this city and the monsoon India.

The availability of simultaneous and continuous measurements of CO_2 and CO have made it possible to study their correlations during different times of the day and during different seasons. The minimum value of slope and correlation coefficient of 0.8 ± 0.2 ppb ppm^{-1} and 0.62 respectively are observed in monsoon. During other three seasons, the slopes vary in narrow range (Table 4) and indicate about the common emission sources of CO during these seasons. These slopes lie in the range (10–15 ppb ppm^{-1}) of anthropogenic sources in developed countries, e.g., Japan. This

ACPD
15, 32185–32238, 2015

suggest that the overall emissions of CO over Ahmedabad are mostly dominated by the anthropogenic (fossil fuel) combustion. These slopes also show significant diurnal variability having lower values (about 5–20 ppb ppm^{-1}) during noon hours and higher values (about 30–50 ppb ppm^{-1}) during evening rush hours with highest correlation ($r > 0.9$). This diurnal pattern is similar to the traffic density and indicate the strong influence of vehicular emissions in the diurnal pattern of CO. Further, using the slope from the evening rush hours (18:00–22:00 IST) data as vehicular emission ratios, the contributions of vehicular emissions and biospheric emissions in the diurnal cycle of CO_2 have been segregated. At rush hours, this analysis suggests that 90–95 % of the total emissions of CO_2 are contributed by vehicular emissions. Using the relationship, the CO emission from Ahmedabad has been estimated. In this estimation, fossil fuel derived emission of CO_2 from EDGAR v4.2 inventory is extrapolated linearly from 2008 to 2014 and it is assumed that there are no year-to-year variations in the land biotic and oceanic CO_2 emissions. The estimated annual emission CO for Ahmedabad is estimated to be 69.2 ± 0.7 Gg for the year of 2014. The extrapolated CO emission from EDGAR inventory for 2014 shows a value smaller than this estimate by about 52 %.

The observed results of CO_2 are also compared with an atmospheric general circulation model based chemistry transport model simulated CO_2 concentrations. The model captures some basic features like the trend of diurnal amplitude, seasonal amplitude etc, qualitatively but not quantitatively. The model captures the seasonal cycle fairly good but the amplitude is very less as compared to the observations. Similarly, performance of the model capturing the change in monthly averaged diurnal amplitude is quiet good ($r = 0.72$), however the slope is very poor. We also examined the correlation between the hourly averaged observed CO_2 and tracer of fossil fuel from model simulation and found fairly good correlation between them. However, no significant correlation has been observed between observed CO_2 and biospheric tracer. It suggests that the levels of CO_2 over Ahmedabad are mostly controlled by the fossil fuel combustion throughout the year.

ACPD
15, 32185–32238, 2015

This work demonstrates the usefulness of simultaneous measurements of CO_2 and CO in an urban region. The anthropogenic and biospheric components of CO_2 have been studied from its temporally varying atmospheric concentrations, and validity of "bottom-up" inventory has been assessed. Use of $CO_{exc} : CO_{2exc}$ ratios avoid some of the problems with assumptions that have to be made with modelling. These results represent a major urban region of India and will be helpful in validating emission inventories, chemistry-transport and terrestrial ecosystem models. However, a bigger network of sites is needed to elucidate more accurate distribution of emissions and their source regions, and run continuously over multiple years for tracking the changes associated with anthropogenic activities and emission mitigation policies.

Acknowledgements. We thank PRL and ISROGBP-ATCTM for funding and support. We acknowledge the support of T. K. Sunil Kumar in making the measurements.

References

Ahmadov, R., Gerbig, C., Kretschmer, R., Koerner, S., Neininger, B., Dolman, A. J., and Sarrat, C.: Mesoscale covariance of transport and CO_2 fluxes: evidence from observations and simulations using the WRF-VPRM coupled atmosphere-biosphere model, J. Geophys. Res.-Atmos., 112, D22107, doi:10.1029/2007JD008552, 2007. 32189

Ammoura, L., Xueref-Remy, I., Gros, V., Baudic, A., Bonsang, B., Petit, J.-E., Perrussel, O., Bonnaire, N., Sciare, J., and Chevallier, F.: Atmospheric measurements of ratios between CO_2 and co-emitted species from traffic: a tunnel study in the Paris megacity, Atmos. Chem. Phys., 14, 12871–12882, doi:10.5194/acp-14-12871-2014, 2014. 32189

Andreae, M. O. and Merlet, P.: Emission of trace gases and aerosols from biomass burning, Global Biogeochem. Cy., 15, 955–966, doi:10.1029/2000GB001382, 2001. 32188, 32224

Baker, A. K., Schuck, T. J., Brenninkmeijer, C. A. M., Rauthe-Schöch, A., Slemr, F., van Velthoven, P. F. J., and Lelieveld, J.: Estimating the contribution of monsoon-related biogenic production to methane emissions from South Asia using CARIBIC observations, Geophys. Res. Lett., 39, L10813, doi:10.1029/2012GL051756, 2012. 32197

Ballav, S., Patra, P. K., Takigawa, M., Ghosh, S., De, U. K., Maksyutov, S., Murayama, S., Mukai, H., and Hashimoto, S.: Simulation of CO_2 Concentration over East Asia Us-

ACPD
15, 32185–32238, 2015

ing the Regional Transport Model WRF-CO2, J. Meteorol. Soc. Jpn., 90, 959–976, doi:10.2151/jmsj.2012-607, 2012. 32210
Ballav, S., Patra, P. K., Sawa, Y., Matsueda, H., Adachi, A., Onogi, S., Takigawa, M., and De, U.: Simulation of CO_2 concentrations at Tsukuba tall tower using WRF–CO_2 tracer transport model, J. Earth System Sci., in press, 2015. 32189
Bhattacharya, S. K., Borole, D. V., Francey, R. J., Allison, C. E., Steele, L. P., Krummel, P., Langenfelds, R., Masarie, K. A., Tiwari, Y. K., and Patra, P.: Trace gases and CO_2 isotope records from Cabo de Rama, India, Curr. Sci. India, 97, 1336–1344, 2009. 32189, 32198
Bitter, M., Ball, S. M., Povey, I. M., and Jones, R. L.: A broadband cavity ringdown spectrometer for in-situ measurements of atmospheric trace gases, Atmos. Chem. Phys., 5, 2547–2560, doi:10.5194/acp-5-2547-2005, 2005. 32192
Boden, T., Marland, G., and Andres, R.: Global, Regional, and National Fossil-Fuel CO_2 Emissions, Oak Ridge, Tenn., USA, doi:10.3334/CDIAC/00001_V2013, 2015. 32188
Brenninkmeijer, C. A. M., Crutzen, P., Boumard, F., Dauer, T., Dix, B., Ebinghaus, R., Filippi, D., Fischer, H., Franke, H., Frieß, U., Heintzenberg, J., Helleis, F., Hermann, M., Kock, H. H., Koeppel, C., Lelieveld, J., Leuenberger, M., Martinsson, B. G., Miemczyk, S., Moret, H. P., Nguyen, H. N., Nyfeler, P., Oram, D., O'Sullivan, D., Penkett, S., Platt, U., Pupek, M., Ramonet, M., Randa, B., Reichelt, M., Rhee, T. S., Rohwer, J., Rosenfeld, K., Scharffe, D., Schlager, H., Schumann, U., Slemr, F., Sprung, D., Stock, P., Thaler, R., Valentino, F., van Velthoven, P., Waibel, A., Wandel, A., Waschitschek, K., Wiedensohler, A., Xueref-Remy, I., Zahn, A., Zech, U., and Ziereis, H.: Civil Aircraft for the regular investigation of the atmosphere based on an instrumented container: The new CARIBIC system, Atmos. Chem. Phys., 7, 4953–4976, doi:10.5194/acp-7-4953-2007, 2007. 32189
Briber, B. M., Hutyra, L. R., Dunn, A. L., Raciti, S. M., and Munger, J. W.: Variations in Atmospheric CO_2 Mixing Ratios across a Boston, MA Urban to Rural Gradient, Land, 2, 304, doi:10.3390/land2030304, 2013. 32189
Cao, G., Zhang, X., Gong, S., and Zheng, F.: Investigation on emission factors of particulate matter and gaseous pollutants from crop residue burning, J. Environ. Sci., 20, 50–55, doi:10.1016/S1001-0742(08)60007-8, 2008. 32224
Chen, H., Winderlich, J., Gerbig, C., Hoefer, A., Rella, C. W., Crosson, E. R., Van Pelt, A. D., Steinbach, J., Kolle, O., Beck, V., Daube, B. C., Gottlieb, E. W., Chow, V. Y., Santoni, G. W., and Wofsy, S. C.: High-accuracy continuous airborne measurements of greenhouse gases

ACPD
15, 32185–32238, 2015

(CO_2 and CH_4) using the cavity ring-down spectroscopy (CRDS) technique, Atmos. Meas. Tech., 3, 375–386, doi:10.5194/amt-3-375-2010, 2010. 32192, 32193
Ciais, P., Sabine, C., Bala, G., Bopp, L., Brovkin, V., Canadell, J., Chhabra, A., DeFries, R., Galloway, J., Heimann, M., Jones, C., Quere, C., Myneni, R., Piao, S., and Thornton, P.: Carbon and Other Biogeochemical Cycles, Cambridge University Press, Cambridge, UK and New York, NY, USA, doi:10.1017/CBO9781107415324.015, book section 6, 465–570, 2013. 32187
Crosson, E.: A cavity ring-down analyzer for measuring atmospheric levels of methane, carbon dioxide, and water vapor, Appl. Phys. B, 92, 403–408, doi:10.1007/s00340-008-3135-y, 2008. 32193
Dhammapala, R., Claiborn, C., Simpson, C., and Jimenez, J.: Emission factors from wheat and Kentucky bluegrass stubble burning: comparison of field and simulated burn experiments, Atmos. Environ., 41, 1512–1520, doi:10.1016/j.atmosenv.2006.10.008, 2007. 32224
Gurney, K. R., Law, R. M., Denning, A. S., Rayner, P. J., Baker, D., Bousquet, P., Bruhwiler, L., Chen, Y. H., Ciais, P., Fan, S., Fung, I., Gloor, M., Heimann, M., Higuchi, K., John, J., Maki, T., Maksyutov, S., Masarie, K., Peylin, P., Prather, M., Pak, B. C., Randerson, J., Sarmiento, J., Taguchi, S., Takahashi, T., and Yuen, C.: Towards robust regional estimates of CO_2 sources and sinks using atmospheric transport models, Nature, 415, 626–630, doi:10.1038/415626a, 2002. 32187
Kar, J., Bremer, H., Drummond, J. R., Rochon, Y. J., Jones, D. B. A., Nichitiu, F., Zou, J., Liu, J., Gille, J. C., Edwards, D. P., Deeter, M. N., Francis, G., Ziskin, D., and Warner, J.: Evidence of vertical transport of carbon monoxide from Measurements of Pollution in the Troposphere (MOPITT), Geophys. Res. Lett., 31, L23105, doi:10.1029/2004GL021128, 2004. 32197
Karion, A., Sweeney, C., Wolter, S., Newberger, T., Chen, H., Andrews, A., Kofler, J., Neff, D., and Tans, P.: Long-term greenhouse gas measurements from aircraft, Atmos. Meas. Tech., 6, 511–526, doi:10.5194/amt-6-511-2013, 2013. 32192
Lai, S. C., Baker, A. K., Schuck, T. J., van Velthoven, P., Oram, D. E., Zahn, A., Hermann, M., Weigelt, A., Slemr, F., Brenninkmeijer, C. A. M., and Ziereis, H.: Pollution events observed during CARIBIC flights in the upper troposphere between South China and the Philippines, Atmos. Chem. Phys., 10, 1649–1660, doi:10.5194/acp-10-1649-2010, 2010. 32204
Lal, S., Naja, M., and Subbaraya, B.: Seasonal variations in surface ozone and its precursors over an urban site in India, Atmos. Environ., 34, 2713–2724, doi:10.1016/S1352-2310(99)00510-5, 2000. 32203

ACPD
15, 32185–32238, 2015

Lal, S., Chandra, N., and Venkataramani, S.: A study of CO_2 and related trace gases using a laser based technique at an urban site in western India, Curr. Sci. India, in press, 2015. 32190

Law, R. M., Rayner, P. J., Steele, L. P., and Enting, I. G.: Using high temporal frequency data for CO_2 inversions, Global Biogeochem. Cy., 16, 1.1–1.18, doi:10.1029/2001GB001593, 1053, 2002. 32189

Law, R. M., Peters, W., Rödenbeck, C., Aulagnier, C., Baker, I., Bergmann, D. J., Bousquet, P., Brandt, J., Bruhwiler, L., Cameron-Smith, P. J., Christensen, J. H., Delage, F., Denning, A. S., Fan, S., Geels, C., Houweling, S., Imasu, R., Karstens, U., Kawa, S. R., Kleist, J., Krol, M. C., Lin, S.-J., Lokupitiya, R., Maki, T., Maksyutov, S., Niwa, Y., Onishi, R., Parazoo, N., Patra, P. K., Pieterse, G., Rivier, L., Satoh, M., Serrar, S., Taguchi, S., Takigawa, M., Vautard, R., Vermeulen, A. T., and Zhu, Z.: TransCom model simulations of hourly atmospheric CO_2: experimental overview and diurnal cycle results for 2002, Global Biogeochem. Cy., 22, GB3009, doi:10.1029/2007GB003050, 2008. 32195

Le Quéré, C., Moriarty, R., Andrew, R. M., Peters, G. P., Ciais, P., Friedlingstein, P., Jones, S. D., Sitch, S., Tans, P., Arneth, A., Boden, T. A., Bopp, L., Bozec, Y., Canadell, J. G., Chevallier, F., Cosca, C. E., Harris, I., Hoppema, M., Houghton, R. A., House, J. I., Jain, A., Johannessen, T., Kato, E., Keeling, R. F., Kitidis, V., Klein Goldewijk, K., Koven, C., Landa, C. S., Landschützer, P., Lenton, A., Lima, I. D., Marland, G., Mathis, J. T., Metzl, N., Nojiri, Y., Olsen, A., Ono, T., Peters, W., Pfeil, B., Poulter, B., Raupach, M. R., Regnier, P., Rödenbeck, C., Saito, S., Salisbury, J. E., Schuster, U., Schwinger, J., Séférian, R., Segschneider, J., Steinhoff, T., Stocker, B. D., Sutton, A. J., Takahashi, T., Tilbrook, B., van der Werf, G. R., Viovy, N., Wang, Y.-P., Wanninkhof, R., Wiltshire, A., and Zeng, N.: Global carbon budget 2014, Earth Syst. Sci. Data Discuss., 7, 521–610, doi:10.5194/essdd-7-521-2014, 2014. 32187

Levin, I., Kromer, B., Schmidt, M., and Sartorius, H.: A novel approach for independent budgeting of fossil fuel CO_2 over Europe by $^{14}CO_2$ observations, Geophys. Res. Lett., 30, 2194, doi:10.1029/2003GL018477, 2003. 32207

Lin, X., Indira, N. K., Ramonet, M., Delmotte, M., Ciais, P., Bhatt, B. C., Reddy, M. V., Angchuk, D., Balakrishnan, S., Jorphail, S., Dorjai, T., Mahey, T. T., Patnaik, S., Begum, M., Brenninkmeijer, C., Durairaj, S., Kirubagaran, R., Schmidt, M., Swathi, P. S., Vinithkumar, N. V., Yver Kwok, C., and Gaur, V. K.: Long-lived atmospheric trace gases measure-

ACPD
15, 32185–32238, 2015

ments in flask samples from three stations in India, Atmos. Chem. Phys., 15, 9819–9849, doi:10.5194/acp-15-9819-2015, 2015. 32188, 32189, 32198, 32199, 32204

Lopez, M., Schmidt, M., Delmotte, M., Colomb, A., Gros, V., Janssen, C., Lehman, S. J., Mondelain, D., Perrussel, O., Ramonet, M., Xueref-Remy, I., and Bousquet, P.: CO, NO_x and $^{13}CO_2$ as tracers for fossil fuel CO_2: results from a pilot study in Paris during winter 2010, Atmos. Chem. Phys., 13, 7343–7358, doi:10.5194/acp-13-7343-2013, 2013. 32189, 32207

Machida, T., Matsueda, H., Sawa, Y., Nakagawa, Y., Hirotani, K., Kondo, N., Goto, K., Nakazawa, T., Ishikawa, K., and Ogawa, T.: Worldwide measurements of atmospheric CO_2 and other trace gas species using commercial airlines, J. Atmos. Ocean. Tech., 25, 1744–1754, doi:10.1175/2008JTECHA1082.1, 2008. 32189

Mahesh, P., Sharma, N., Dadhwal, V., Rao, P., Apparao, B., Ghosh, A., Mallikarjun, K., and Ali, M.: Impact of land-sea breeze and rainfall on CO_2 variations at a coastal station, Journal of Earth Science and Climatic Change, 5, 201, doi:10.4172/2157-7617.1000201, 2014. 32189

Mallik, C., Lal, S., and Venkataramani, S.: Trace gases at a semi-arid urban site in western India: variability and inter-correlations, J. Atmos. Chem., 72, 143–164, doi:10.1007/s10874-015-9311-7, 2015. 32190

Newman, S., Jeong, S., Fischer, M. L., Xu, X., Haman, C. L., Lefer, B., Alvarez, S., Rappenglueck, B., Kort, E. A., Andrews, A. E., Peischl, J., Gurney, K. R., Miller, C. E., and Yung, Y. L.: Diurnal tracking of anthropogenic CO_2 emissions in the Los Angeles basin megacity during spring 2010, Atmos. Chem. Phys., 13, 4359–4372, doi:10.5194/acp-13-4359-2013, 2013. 32188, 32207

Olsen, S. C. and Randerson, J. T.: Differences between surface and column atmospheric CO_2 and implications for carbon cycle research, J. Geophys. Res.-Atmos., 109, d02301, doi:10.1029/2003JD003968, 2004. 32195

Onogi, K., Tsutsui, J., Koide, H., Sakamoto, M., Kobayashi, S., Hatsushika, H., Matsumoto, T., Yamazaki, N., Kamahori, H., Takahashi, K., Kadokura, S., Wada, K., Kato, K., Oyama, R., Ose, T., Mannoji, N., and Taira, R.: The JRA-25 reanalysis, J. Meteorol. Soc. Jpn., 85, 369–432, doi:10.2151/jmsj.85.369, 2007. 32194

Park, M., Randel, W. J., Emmons, L. K., and Livesey, N. J.: Transport pathways of carbon monoxide in the Asian summer monsoon diagnosed from Model of Ozone and Related Tracers (MOZART), J. Geophys. Res.-Atmos., 114, D08303, doi:10.1029/2008JD010621, 2009. 32197

ACPD
15, 32185–32238, 2015

Patra, P. K., Law, R. M., Peters, W., Rödenbeck, C., Takigawa, M., Aulagnier, C., Baker, I., Bergmann, D. J., Bousquet, P., Brandt, J., Bruhwiler, L., Cameron-Smith, P. J., Christensen, J. H., Delage, F., Denning, A. S., Fan, S., Geels, C., Houweling, S., Imasu, R., Karstens, U., Kawa, S. R., Kleist, J., Krol, M. C., Lin, S.-J., Lokupitiya, R., Maki, T., Maksyutov, S., Niwa, Y., Onishi, R., Parazoo, N., Pieterse, G., Rivier, L., Satoh, M., Serrar, S., Taguchi, S., Vautard, R., Vermeulen, A. T., and Zhu, Z.: TransCom model simulations of hourly atmospheric CO_2: analysis of synoptic-scale variations for the period 2002–2003, Global Biogeochem. Cy., 22, GB4013, doi:10.1029/2007GB003081, 2008. 32195

Patra, P. K., Niwa, Y., Schuck, T. J., Brenninkmeijer, C. A. M., Machida, T., Matsueda, H., and Sawa, Y.: Carbon balance of South Asia constrained by passenger aircraft CO_2 measurements, Atmos. Chem. Phys., 11, 4163–4175, doi:10.5194/acp-11-4163-2011, 2011. 32189, 32197, 32198, 32201, 32210, 32211, 32238

Patra, P. K., Canadell, J. G., Houghton, R. A., Piao, S. L., Oh, N.-H., Ciais, P., Manjunath, K. R., Chhabra, A., Wang, T., Bhattacharya, T., Bousquet, P., Hartman, J., Ito, A., Mayorga, E., Niwa, Y., Raymond, P. A., Sarma, V. V. S. S., and Lasco, R.: The carbon budget of South Asia, Biogeosciences, 10, 513–527, doi:10.5194/bg-10-513-2013, 2013. 32187, 32189

Pérez-Landa, G., Ciais, P., Gangoiti, G., Palau, J. L., Carrara, A., Gioli, B., Miglietta, F., Schumacher, M., Millán, M. M., and Sanz, M. J.: Mesoscale circulations over complex terrain in the Valencia coastal region, Spain – Part 2: Modeling CO_2 transport using idealized surface fluxes, Atmos. Chem. Phys., 7, 1851–1868, doi:10.5194/acp-7-1851-2007, 2007. 32189

Peylin, P., Law, R. M., Gurney, K. R., Chevallier, F., Jacobson, A. R., Maki, T., Niwa, Y., Patra, P. K., Peters, W., Rayner, P. J., Rödenbeck, C., van der Laan-Luijkx, I. T., and Zhang, X.: Global atmospheric carbon budget: results from an ensemble of atmospheric CO_2 inversions, Biogeosciences, 10, 6699–6720, doi:10.5194/bg-10-6699-2013, 2013. 32187

Popa, M. E., Vollmer, M. K., Jordan, A., Brand, W. A., Pathirana, S. L., Rothe, M., and Röckmann, T.: Vehicle emissions of greenhouse gases and related tracers from a tunnel study: $CO : CO_2$, $N_2O : CO_2$, $CH_4 : CO_2$, $O_2 : CO_2$ ratios, and the stable isotopes ^{13}C and ^{18}O in CO_2 and CO, Atmos. Chem. Phys., 14, 2105–2123, doi:10.5194/acp-14-2105-2014, 2014. 32188

Randel, W. J. and Park, M.: Deep convective influence on the Asian summer monsoon anticyclone and associated tracer variability observed with Atmospheric Infrared Sounder (AIRS), J. Geophys. Res.-Atmos., 111, D12314, doi:10.1029/2005JD006490, 2006. 32197

ACPD
15, 32185–32238, 2015

Randerson, J. T., Thompson, M. V., Conway, T. J., Fung, I. Y., and Field, C. B.: The contribution of terrestrial sources and sinks to trends in the seasonal cycle of atmospheric carbon dioxide, Global Biogeochem. Cy., 11, 535–560, doi:10.1029/97GB02268, 1997. 32194

Russo, R. S., Talbot, R. W., Dibb, J. E., Scheuer, E., Seid, G., Jordan, C. E., Fuelberg, H. E., Sachse, G. W., Avery, M. A., Vay, S. A., Blake, D. R., Blake, N. J., Atlas, E., Fried, A., Sandholm, S. T., Tan, D., Singh, H. B., Snow, J., and Heikes, B. G.: Chemical composition of Asian continental outflow over the western Pacific: results from Transport and Chemical Evolution over the Pacific (TRACE-P), J. Geophys. Res.-Atmos., 108, 8804, doi:10.1029/2002JD003184, 2003. 32204

Sánchez-Ccoyllo, O., Ynoue, R., Martins, L., Astolfo, R., Miranda, R., Freitas, E., Borges, A., Fornaro, A., Freitas, H., Moreira, A., and Andrade, M.: Vehicular particulate matter emissions in road tunnels in Sao Paulo, Brazil, Environ. Monit. Assess., 149, 241–249, doi:10.1007/s10661-008-0198-5, 2009. 32224

Schuck, T. J., Brenninkmeijer, C. A. M., Baker, A. K., Slemr, F., von Velthoven, P. F. J., and Zahn, A.: Greenhouse gas relationships in the Indian summer monsoon plume measured by the CARIBIC passenger aircraft, Atmos. Chem. Phys., 10, 3965–3984, doi:10.5194/acp-10-3965-2010, 2010. 32189

Schuck, T. J., Ishijima, K., Patra, P. K., Baker, A. K., Machida, T., Matsueda, H., Sawa, Y., Umezawa, T., Brenninkmeijer, C. A. M., and Lelieveld, J.: Distribution of methane in the tropical upper troposphere measured by CARIBIC and CONTRAIL aircraft, J. Geophys. Res.-Atmos., 117, D19304, doi:10.1029/2012JD018199, 2012. 32189

Sharma, N., Dadhwal, V., Kant, Y., Mahesh, P., Mallikarjun, K., Gadavi, H., Sharma, A., and Ali, M.: Atmospheric CO_2 variations in two contrasting environmental sites over India, Air, Soil and Water Res., 7, 61–68, doi:10.4137/ASWR.S13987, 2014. 32189, 32201

Streets, D. G., Bond, T. C., Carmichael, G. R., Fernandes, S. D., Fu, Q., He, D., Klimont, Z., Nelson, S. M., Tsai, N. Y., Wang, M. Q., Woo, J.-H., and Yarber, K. F.: An inventory of gaseous and primary aerosol emissions in Asia in the year 2000, J. Geophys. Res.-Atmos., 108, 8809, doi:10.1029/2002JD003093, 2003. 32224

Suntharalingam, P., Jacob, D. J., Palmer, P. I., Logan, J. A., Yantosca, R. M., Xiao, Y., Evans, M. J., Streets, D. G., Vay, S. L., and Sachse, G. W.: Improved quantification of Chinese carbon fluxes using CO_2 / CO correlations in Asian outflow, J. Geophys. Res.-Atmos., 109, D18S18, doi:10.1029/2003JD004362, 2004. 32204

ACPD
15, 32185–32238, 2015

Takahashi, T., Sutherland, S. C., Wanninkhof, R., Sweeney, C., Feely, R. A., Chipman, D. W., Hales, B., Friederich, G., Chavez, F., Sabine, C., Watson, A., Bakker, D. C., Schuster, U., Metzl, N., Yoshikawa-Inoue, H., Ishii, M., Midorikawa, T., Nojiri, Y., Körtzinger, A., Steinhoff, T., Hoppema, M., Olafsson, J., Arnarson, T. S., Tilbrook, B., Johannessen, T., Olsen, A., Bellerby, R., Wong, C., Delille, B., Bates, N., and de Baar, H. J.: Climatological mean and decadal change in surface ocean pCO_2, and net sea–air CO_2 flux over the global oceans, Deep-Sea Res. Pt. II, 56, 554–577, doi:10.1016/j.dsr2.2008.12.009, 2009. 32194

Takegawa, N., Kondo, Y., Koike, M., Chen, G., Machida, T., Watai, T., Blake, D. R., Streets, D. G., Woo, J.-H., Carmichael, G. R., Kita, K., Miyazaki, Y., Shirai, T., Liley, J. B., and Ogawa, T.: Removal of NO_x and NO_y in Asian outflow plumes: aircraft measurements over the western Pacific in January 2002, J. Geophys. Res.-Atmos., 109, D23S04, doi:10.1029/2004JD004866, 2004. 32204

Tiwari, Y. K., Vellore, R. K., Kumar, K. R., van der Schoot, M., and Cho, C.-H.: Influence of monsoons on atmospheric CO_2 spatial variability and ground-based monitoring over India, Sci. Total Environ., 490, 570–578, doi:10.1016/j.scitotenv.2014.05.045, 2014. 32189, 32198

Turnbull, J. C., Miller, J. B., Lehman, S. J., Tans, P. P., Sparks, R. J., and Southon, J.: Comparison of $^{14}CO_2$, CO, and SF_6 as tracers for recently added fossil fuel CO_2 in the atmosphere and implications for biological CO_2 exchange, Geophys. Res. Lett., 33, L01817, doi:10.1029/2005GL024213, 2006. 32187, 32188, 32207

Turnbull, J. C., Karion, A., Fischer, M. L., Faloona, I., Guilderson, T., Lehman, S. J., Miller, B. R., Miller, J. B., Montzka, S., Sherwood, T., Saripalli, S., Sweeney, C., and Tans, P. P.: Assessment of fossil fuel carbon dioxide and other anthropogenic trace gas emissions from airborne measurements over Sacramento, California in spring 2009, Atmos. Chem. Phys., 11, 705–721, doi:10.5194/acp-11-705-2011, 2011. 32207

Vogel, F. R., Hammer, S., Steinhof, A., Kromer, B., and Levin, I.: Implication of weekly and diurnal ^{14}C calibration on hourly estimates of CO-based fossil fuel CO_2 at a moderately polluted site in southwestern Germany, Tellus B, 62, 512–520, doi:10.1111/j.1600-0889.2010.00477.x, 2010. 32207

Wada, A., Matsueda, H., Sawa, Y., Tsuboi, K., and Okubo, S.: Seasonal variation of enhancement ratios of trace gases observed over 10 years in the western North Pacific, Atmos. Environ., 45, 2129–2137, doi:10.1016/j.atmosenv.2011.01.043, 2011. 32204

Wang, Y., Munger, J. W., Xu, S., McElroy, M. B., Hao, J., Nielsen, C. P., and Ma, H.: CO_2 and its correlation with CO at a rural site near Beijing: implications for combustion efficiency in

ACPD
15, 32185–32238, 2015

China, Atmos. Chem. Phys., 10, 8881–8897, doi:10.5194/acp-10-8881-2010, 2010. 32187, 32188

Welp, L. R., Keeling, R. F., Weiss, R. F., Paplawsky, W., and Heckman, S.: Design and performance of a Nafion dryer for continuous operation at CO_2 and CH_4 air monitoring sites, Atmos. Meas. Tech., 6, 1217–1226, doi:10.5194/amt-6-1217-2013, 2013. 32193

Westerdahl, D., Wang, X., Pan, X., and Zhang, K. M.: Characterization of on-road vehicle emission factors and microenvironmental air quality in Beijing, China, Atmos. Environ., 43, 697–705, doi:10.1016/j.atmosenv.2008.09.042, 2009. 32224

Wong, K. W., Fu, D., Pongetti, T. J., Newman, S., Kort, E. A., Duren, R., Hsu, Y.-K., Miller, C. E., Yung, Y. L., and Sander, S. P.: Mapping $CH_4 : CO_2$ ratios in Los Angeles with CLARS-FTS from Mount Wilson, California, Atmos. Chem. Phys., 15, 241–252, doi:10.5194/acp-15-241-2015, 2015. 32205

Wunch, D., Wennberg, P. O., Toon, G. C., Keppel-Aleks, G., and Yavin, Y. G.: Emissions of greenhouse gases from a North American megacity, Geophys. Res. Lett., 36, L15810, doi:10.1029/2009GL039825, 2009. 32188, 32205

ACPD
15, 32185–32238, 2015

Table 1. Emission ratios of CO/CO_2 (ppb ppm^{-1}), derived from emission factors (gram of gases emitted per kilogram of fuel burned).

Biomass burning	Transport		Industry	Domestic	
Crop-residue[a,b,c]	Diesel[d,e,f]	Gasoline[d,f]	Coal	Coal[d,f]	Biofuel[c,d]
45.7–123.6	8.6–65.2	33.5	23.5–40.4	53.3–62.2	52.9–98.5

[a] Dhammapala et al. (2007). [b] Cao et al. (2008). [c] Andreae and Merlet (2001). [d] Streets et al. (2003). [e] Sánchez-Ccoyllo et al. (2009). [f] Westerdahl et al. (2009).

ACPD
15, 32185–32238, 2015

Table 2. Estimates of emissions of CO using the the CO_2 emission from EDGAR inventory over the box (72.3 < longitude < 72.7° E, 22.8 < latitude < 23.2° N) and observed $CO_{exc} : CO_{2exc}$ slopes for different time periods. The correlation coefficient for corresponding slopes are given inside the bracket in slope column. Monsoon data are not included for calculating slopes.

Time (IST)	Slope (ppb ppm^{-1}) Correlation coefficient (r)	EDGAR Emissions (Gg yr^{-1}) CO_2	 CO	Estimated Emssions Gg (yr)
23:00–05:00 IST	13 ± 0.14 (0.84)			69.2 ± 0.7
06:00–10:00 IST	11.4 ± 0.19 (0.75)			60.7 ± 1.0
11:00–16:00 IST	14.9 ± 0.19 (0.78)	8368.6	45.3	79.3 ± 1.0
18:00–05:00 IST	34.6 ± 0.37 (0.76)			184.2 ± 1.9
Full day (24 h)	10.8 ± 0.09 (0.73)			57.5 ± 0.5

ACPD
15, 32185–32238, 2015

Table 3. Model performance matrices used to quantify the level of agreement between model simulations and observations. These statistics are based on hourly values in each day.

Parameter	Winter	Autumn	Monsoon	All months
MB (ppm)	−2.72	12.64	−2.45	2.27
FGE (%)	0.96	3.12	2.0	1.76
RMSE (ppm)	5.21	12.82	9.14	8.60
RMSE (%)	1.27	3.21	2.20	2.09

ACPD
15, 32185–32238, 2015

Table 4. Summary of results for the study period. The total refers to the average of all the 24 h data while noon time values refer to the average for 12:00–16:00 IST. The "exc" refer to the excess concentrations of CO_2 and CO after subtracting the background concentrations.

Period	Mean (ppm)		Diurnal amplitude (ppm)		Correlation $CO_{exc} : CO_{2exc}$	
	CO_2	CO	CO_2	CO	Slope (ppb ppm^{-1})	Correlation coefficient (r)
Monsoon	400.3 ± 6.8	0.19 ± 0.13	12.4	0.24	0.6 ± 0.1	0.62
Autumn	419.6 ± 22.8	0.72 ± 0.71	40.9	1.36	8.5 ± 0.2	0.72
Winter	417.2 ± 18.5	0.73 ± 0.68	31.7	1.01	12.7 ± 0.2	0.71
Spring	415.4 ± 14.8	0.41 ± 0.40	15.9	0.62	8.4 ± 0.1	0.87
Annual	413.0 ± 13.7	0.50 ± 0.37	25.0	0.48	8.3 ± 0.7	0.79

ACPD
15, 32185–32238, 2015

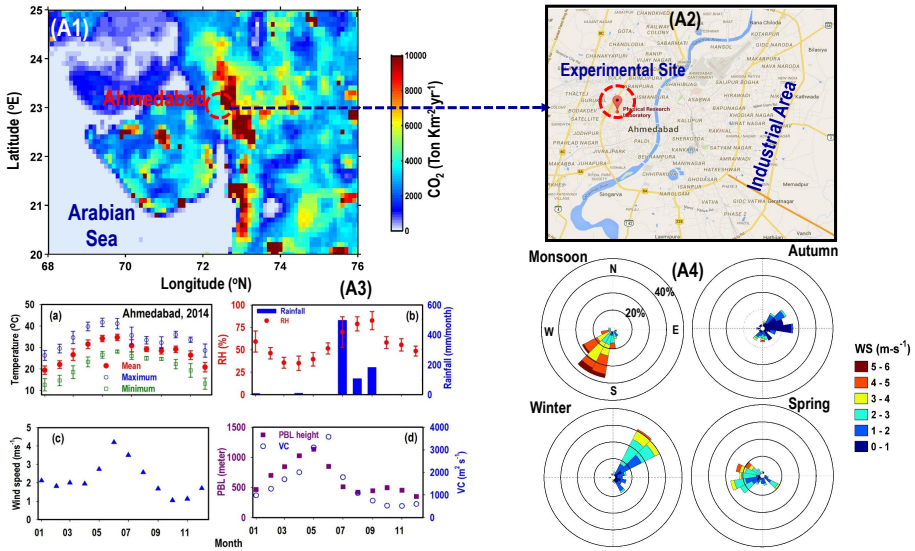

Figure 1. (A1) Spatial distribution of total anthropogenic CO_2 emissions from EDGARv4.2 inventory over Ahmedabad and surrounding regions. (A2) The Ahmedabad city map showing location of the experimental site (PRL). (A3: **a**–**d**) Monthly average temperature with monthly maximum and minimum value, relative humidity (RH), rainfall, wind speed, PBL height and ventilation coefficient (VC) over Ahmedabad during the year 2014. Temperature, RH and wind speed are taken from the Wunderground weather (www.wunderground.com) while rainfall and PBLH data are used from Tropical Rainfall Measuring Mission (TRMM) satellite and MEERA reanalysis data. (A4) Wind rose plots for Ahmedabad for the four seasons of 2014 using daily average data from the Wunderground.

ACPD
15, 32185–32238, 2015

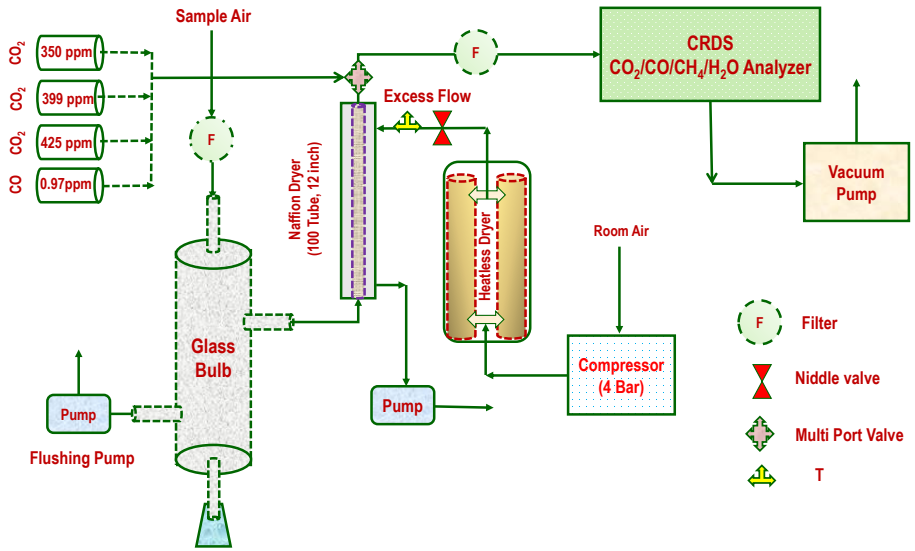

Figure 2. Schematic diagram of the analysis system. We introduced additionally a Nafion dryer in the inlet of instrument for removing the water vapour from the ambient air. The calibration mixtures (three) from NOAA, USA are used to calibrate CO_2 measurements and one calibration mixture from Linde, UK is used to calibrate CO measurements.

ACPD
15, 32185–32238, 2015

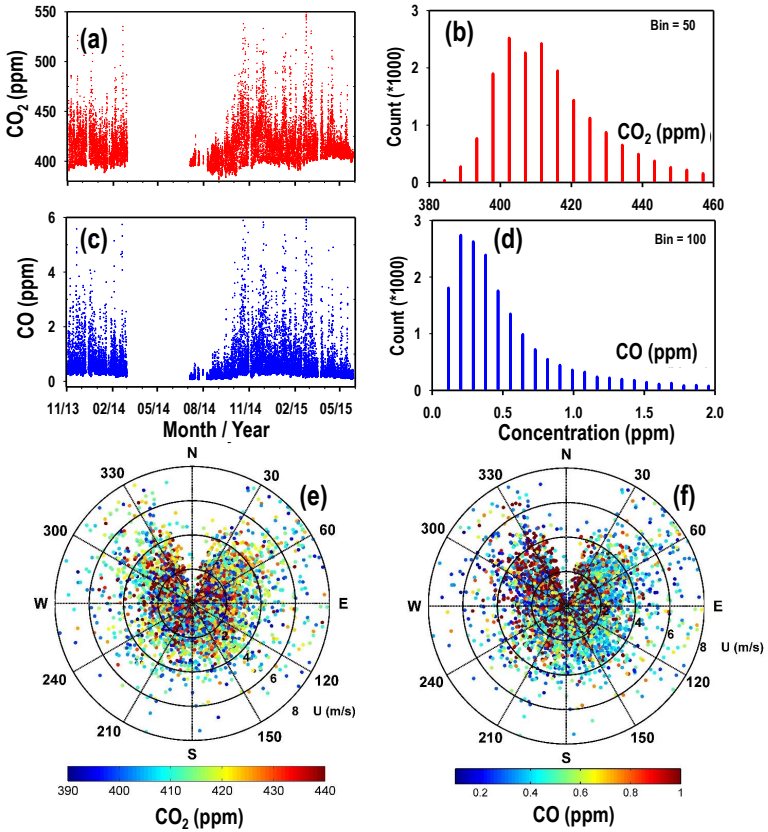

Figure 3. (a, c) Time series of 30 min average values CO_2 and CO measured at Ahmedabad for the study period. **(b, d)** The frequency distribution in CO_2 and CO concentrations for the study period using 30 min mean of both gases. **(e, f)** The polar plots show the variation of 30 min averaged CO_2 and CO at this site with wind direction and speed during the study period except July, August and September due to unavailability of meteorology data.

ACPD
15, 32185–32238, 2015

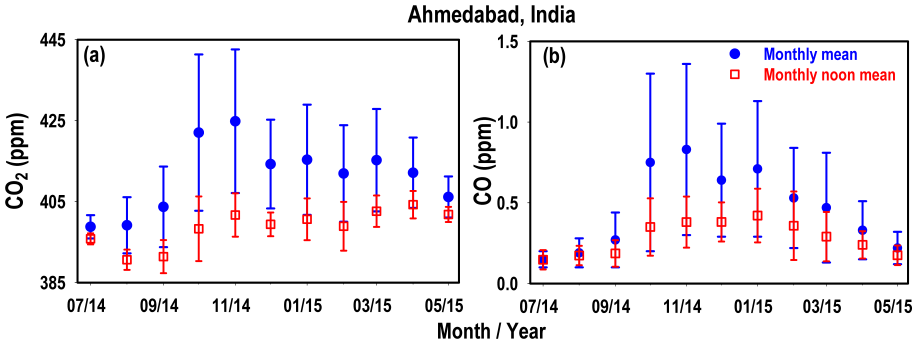

Figure 4. The seasonal variation of CO_2 and CO at Ahmedabad, India from July 2014 to May 2015 using their monthly mean concentrations. The blue dots and red rectangles show the monthly average concentrations of these gases for the total (00:00–24:00 IST) and noon time (12:00–16:00 IST) data respectively with 1σ spread. All times are in Indian Standard Time (IST), which is 5.5 h ahead of GMT.

ACPD
15, 32185–32238, 2015

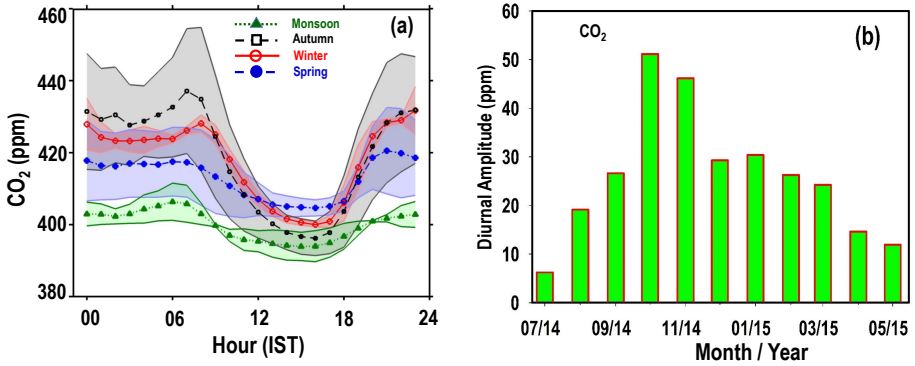

Figure 5. (a) Average diurnal variation of CO_2 over Ahmedabad during all the four seasons. **(b)** Monthly variation of average diurnal amplitude of CO_2 from July 2014 to May 2015.

ACPD
15, 32185–32238, 2015

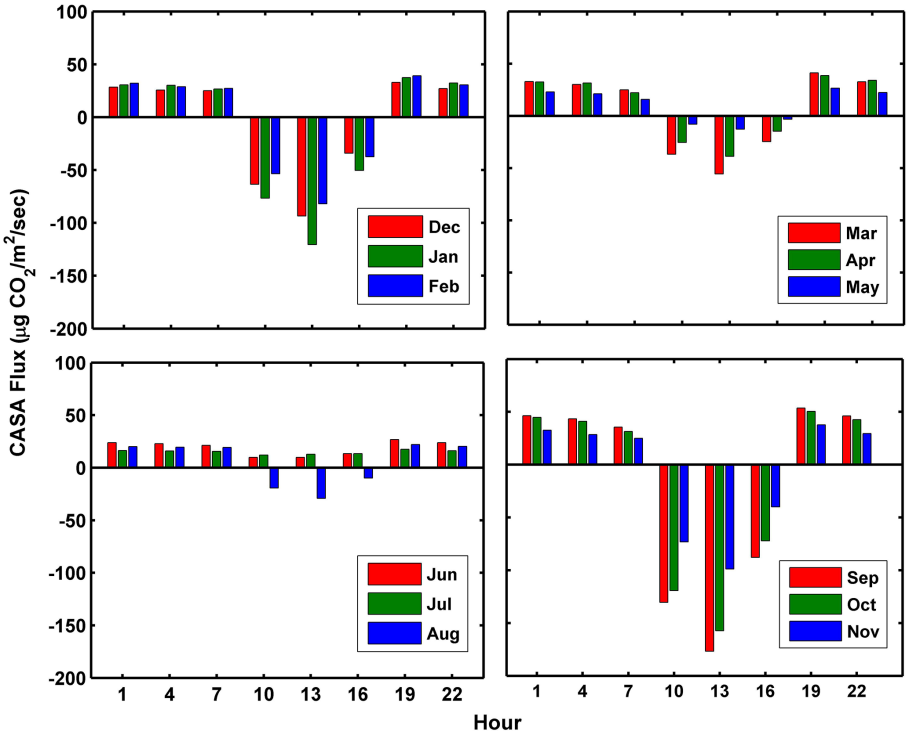

Figure 6. Diurnal variation of biospheric fluxes from the CASA ecosystem model.

ACPD
15, 32185–32238, 2015

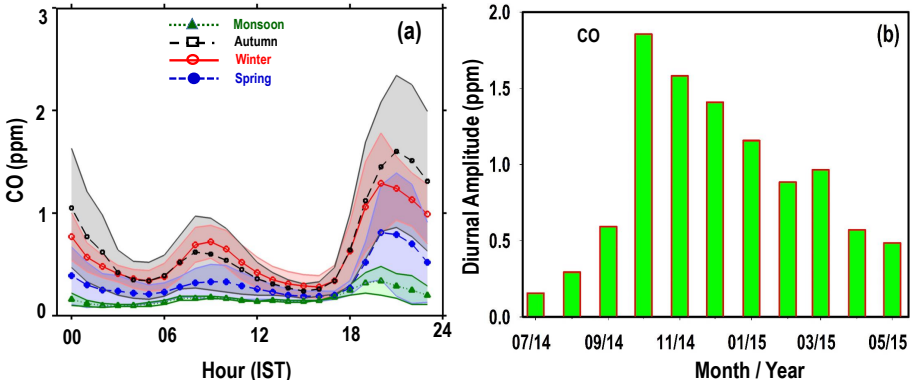

Figure 7. (a) Diurnal variation of CO over Ahmedabad during all the four seasons. **(b)** Monthly variation of the diurnal amplitude of CO.

ACPD
15, 32185–32238, 2015

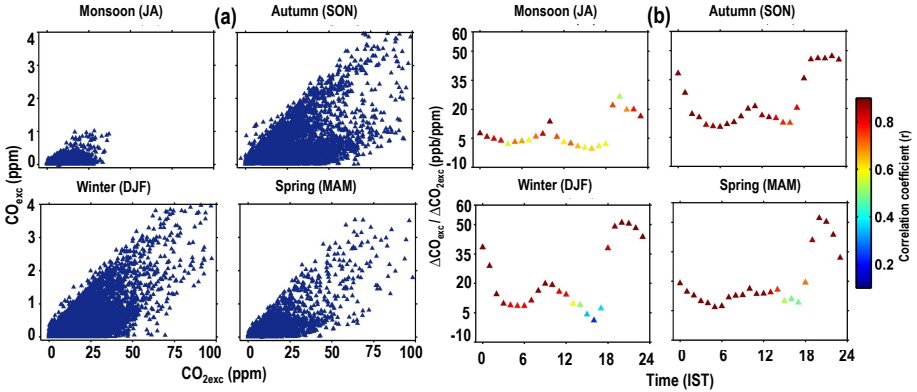

Figure 8. (a) Correlation of excess CO above background (CO_{exc}) with the excess CO_2 above background (CO_{2exc}) during all the four different seasons. Each data points are averaged for 30 min. **(b)** The diurnal variation of the $\Delta CO_{exc}/\Delta CO_{exc}$ slopes during all the four seasons. The colour bar in this plot shows the correlation coefficient (r) for corresponding time.

ACPD
15, 32185–32238, 2015

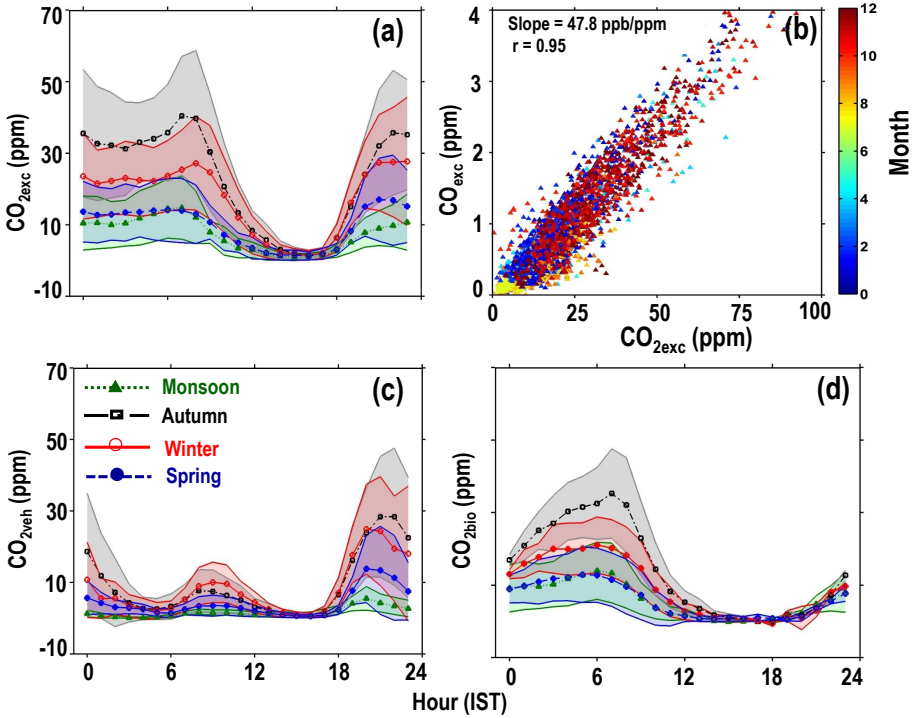

Figure 9. (a) Diurnal cycle of excess CO_2 over background levels during all the four seasons. **(b)** Correlation between excess CO and CO_2 for evening hours (18:00–21:00 IST) during the study period. Contributions of fossil fuel **(c)** and biosphere **(d)** in the diurnal variation of excess CO_2 in all the four seasons.

ACPD
15, 32185–32238, 2015

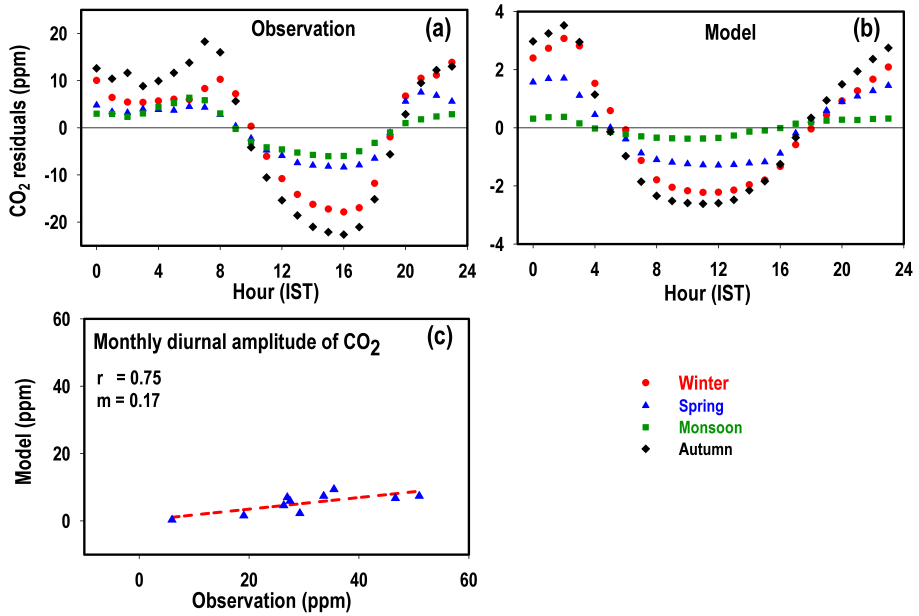

Figure 10. Residual of the diurnal cycle of CO_2 (in ppm) for **(a)** observations and **(b)** modal simulation over Ahmedabad in all the four seasons. Please note that the scales of model and observational diurnal cycles are different. **(c)** Correlation between observed and model simulated monthly mean diurnal cycle amplitudes.

ACPD
15, 32185–32238, 2015

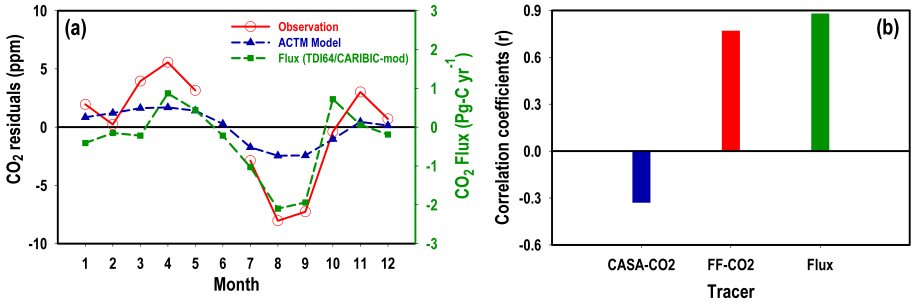

Figure 11. (a) The red circles and blue triangles show the mean seasonal cycles of CO_2 (in ppm) using afternoon values only, calculated from measurements and model over Ahmedabad. The green triangles show the seasonal cycles of CO_2 flux over South Asia, calculated from TDI64/CARIBIC-modified inverse model as given in Patra et al. (2011) (Fig. 3d). **(b)** Blue bar and red bar shows the correlation coefficient (r) of model CO_2 concentration of biospheric tracer and fossil fuel tracer component with observed concentrations of CO_2 taking the entire annual time series of daily mean data, respectively. The green bar shows the correlation coefficient between the monthly residuals of afternoon mean only and the CO_2 flux over South Asia.

ACPD
15, 32185–32238, 2015